geosciences

MDPI

Article

Speleothem Records of the Hydroclimate Variability throughout the Last Glacial Cycle from Manita peć Cave (Velebit Mountain, Croatia)

Maša Surić [1,*], Petra Bajo [2], Robert Lončarić [1], Nina Lončar [1], Russell N. Drysdale [3], John C. Hellstrom [4] and Quan Hua [5]

1 Department of Geography, University of Zadar, 23000 Zadar, Croatia; rloncar@unizd.hr (R.L.); nloncar@unizd.hr (N.L.)
2 Croatian Geological Survey, 10000 Zagreb, Croatia; pbajo@hgi-cgs.hr
3 School of Geography, Faculty of Science, The University of Melbourne, Melbourne, VIC 3010, Australia; rnd@unimelb.edu.au
4 School of Earth Sciences, University of Melbourne, Melbourne, VIC 3053, Australia; j.hellstrom@unimelb.edu.au
5 Australian Nuclear Science and Technology Organisation, Lucas Heights, NSW 2234, Australia; qhx@ansto.gov.au
* Correspondence: msuric@unizd.hr; Tel.: +385-23-345022

Citation: Surić, M.; Bajo, P.; Lončarić, R.; Lončar, N.; Drysdale, R.N.; Hellstrom, J.C.; Hua, Q. Speleothem Records of the Hydroclimate Variability throughout the Last Glacial Cycle from Manita peć Cave (Velebit Mountain, Croatia). *Geosciences* **2021**, *11*, 347. https://doi.org/10.3390/geosciences11080347

Academic Editors: Mohammad Valipour and Jesus Martinez-Frias

Received: 5 July 2021
Accepted: 17 August 2021
Published: 19 August 2021

Abstract: We present stable carbon ($\delta^{13}C$) and oxygen ($\delta^{18}O$) isotope records from two partially coeval speleothems from Manita peć Cave, Croatia. The cave is located close to the Adriatic coast (3.7 km) at an elevation of 570 m a.s.l. The site experienced competing Mediterranean and continental climate influences throughout the last glacial cycle and was situated close to the ice limit during the glacial phases. U-Th dating constrains the growth history from Marine Isotope Stage (MIS) 5 to MIS 3 and the transition from MIS 2 to MIS 1. ^{14}C dating was used to estimate the age of the youngest part of one stalagmite found to be rich in detrital thorium and thus undatable by U-Th. On a millennial scale, $\delta^{18}O$ variations partly mimic the Dansgaard–Oeschger interstadials recorded in Greenland ice cores (Greenland Interstadials, GI) from GI 22 to GI 13. We interpret our $\delta^{18}O$ record as a proxy for variations in precipitation amount and/or moisture sources, and the $\delta^{13}C$ record is interpreted as a proxy for changes in soil bioproductivity. The latter indicates a generally reduced vegetation cover towards MIS 3–MIS 4, with shifts of ~8‰ and approaching values close to those of the host rock. However, even during the coldest phases, when a periglacial setting and enhanced aridity sustained long-residence-time groundwater, carbonic-acid dissolution remains the driving force of the karstification processes. Speleothem morphology follows changes in environmental conditions and complements regional results of submerged speleothems findings. Specifically, narrow sections of light porous spelaean calcite precipitated during the glacial/stadial sea-level lowstands, while the warmer and wetter conditions were marked with compact calcite and hiatuses in submerged speleothems due to sea-level highstands. Presumably, the transformation of this littoral site to a continental one with somewhat higher amounts of orographic precipitation was a site-specific effect that masked regional environmental changes.

Keywords: speleothem; cave; hydroclimate; palaeoenvironmental changes; Croatia

1. Introduction

The last glacial cycle, as revealed from Greenland ice cores [1,2], was marked by a series of rapid, millennial-scale climate oscillations known as Dansgaard–Oeschger (DO) cycles [1]. In total, 25 such cycles show a sawtooth pattern of abrupt increase in temperature and humidity, referred to as Greenland Interstadials (GI), and relatively slow gradual cooling, which led to dry and cold Greenland Stadials (GS) [3,4]. These oscillations

have been documented in various terrestrial and marine records, particularly their climate-driven isotopic ($\delta^{18}O$ and $\delta^{13}C$) variations. The timing and duration of certain events substantially differ in various archives, among which radiometrically dated speleothems appear to be very valuable material due to their absolute dating of high precision and accuracy [5].

Provided the deposition of spelaean calcite occurs in isotopic equilibrium with dripwater, speleothem $\delta^{18}O$ variations are governed solely by dripwater $\delta^{18}O$ and cave temperature [6]. Cave temperature is usually thought to be stable and to reflect the mean annual air temperature (MAAT) of the surface [7], but dripwater $\delta^{18}O$ depends on numerous factors affecting meteoric water on its way from the vapour source via the atmosphere, soil and epikarst to the drip site in the cave, such as altitude, latitude, continentality and rainfall amount [8]. Consequently, the dominant influence on speleothem $\delta^{18}O$ is strictly site-specific. In the Mediterranean, rainfall amount is the dominant factor controlling speleothem $\delta^{18}O$ in Spain [9–12], Portugal [13,14], Italy [15–25], Croatia [26–29], Greece [30,31] and Israel [32–34]. These speleothem records are characterized by $\delta^{18}O$ decreases at times of increased precipitation amount, associated with generally warm and humid periods; higher $\delta^{18}O$ values are thus related to dry and cold conditions. On the other hand, temperature-controlled $\delta^{18}O$ signals, as reconstructed from Greenland ice cores [2], revealed in six caves along the 475 km-long transect of the northern rim of the European Alps [4,35–39], but also in Turkey [40], Ireland [41] and Belgium [42], that decreased $\delta^{18}O$ represents cold stadials and increased values mark warm interstadials. Along with $\delta^{18}O$ variations, stable carbon isotopic composition ($\delta^{13}C$) of spelaean calcite provides insight into climate-controlled environmental changes via its dependence on vegetation cover and soil biogenic activity, which respond to temperature changes and moisture availability [43,44].

The Adriatic Sea, located in the northernmost part of the central Mediterranean, is the contact zone of competing continental European and maritime climate influences. Its eastern Croatian coast, rich in karst features, offers good potential for palaeoenvironmental studies, not only speleothem-based [26–28,45–50] but also based on other proxies and archives [51–57]. Palaeoenvironmental studies concerning sea-level changes, conducted on eastern Adriatic submerged speleothems, revealed speleothem deposition during cold climate phases, apparently even during the Last Glacial Maximum (LGM) [45]. Evidence of more or less interrupted speleothem growth throughout the last glacial cycle is provided also from the Tyrrhenian coast (see review in [58]), Apulia [25] and Israel [32].

Here, we present stable isotope ($\delta^{18}O$ and $\delta^{13}C$) records from two partially coeval speleothems collected from the monitored cave of Manita peć [49] (hereafter MP). It is located in the littoral part of the Croatian Dinaric karst, in the Velebit Mountain, 3.7 km from the coastline. Proxy data from U-Th- and ^{14}C-dated stalagmites enable partial reconstruction of environmental changes during the last 110 ka. Given the cave's position between the Mediterranean and continental Europe, we compare our results with concurrent Mediterranean and Alpine records (Figure 1a) in order to identify the prevailing influences and factors controlling isotopic variations in speleothems, as well as their different intensity and spatiotemporal extent at the regional to local scale.

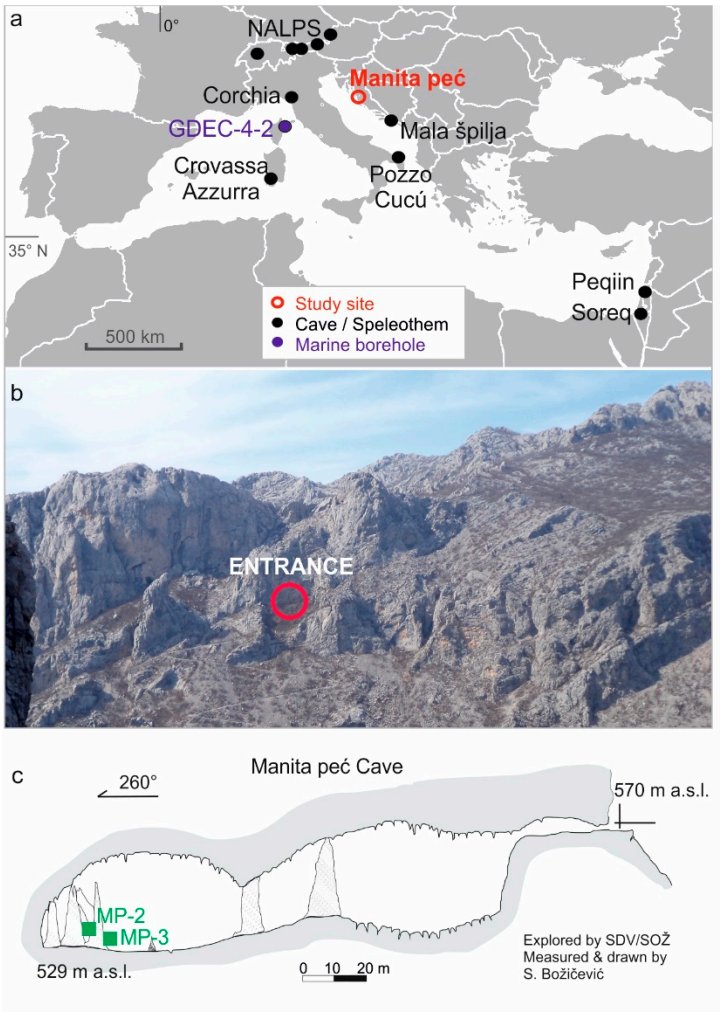

Figure 1. (**a**) Location of Manita peć Cave and other palaeoclimate archives used for comparison: North Alps (NALPS) caves [4,36], Mala špilja Cave [27], Corchia Cave [15], Crovassa Azzurra Cave [24], Pozzo Cucú Cave [25], Soreq and Peqiin caves [33] and marine borehole GDEC-4-2 [59]. The position of NGRIP ice core, which is not shown here, is 75°5′ N, 42°19′ W [2]. (**b**) Cave entrance on the steep and bare side of the Paklenica canyon, Velebit Mountain. (**c**) Cave survey with marked speleothems positions (green squares and IDs).

2. Regional Settings and Study Site

Manita peć Cave (44°18′ N, 15°28′ E) is located at 570 m a.s.l. in the side of the Paklenica canyon carved perpendicularly into the Velebit Mountain. It was formed in Upper Jurassic limestone and consists of simple descending spacious chambers with heights up to 38.5 m. Our study site, where the monitoring was conducted and in which speleothems were collected, was at the end of the cave, 150 m from and 40 m below the entrance level. Presently, the surface is mostly bare karst with sparse grass and shrubs (Figure 1b). The recharge area is limited, and the origin of the cave dripwater is restricted to the local meteoric input due to the cave position in epikarst near the summit and relatively shallow overburden (80 m). The infiltration elevation (i.e., altitude of the catchment) is just slightly above the elevation of the cave.

Owing to the relative vicinity to the Adriatic coast (3.7 km) and the altitude (570 m a.s.l.), the climate type is Cfa—temperate humid climate with hot summers (according to the Köppen–Geiger climate classification [60]), but bordering with Cfb—temperate humid climate with warm summers. The MAAT measured in front of the cave (February 2014–February 2015) was 13.7 °C, while the cave MAAT measured in the innermost part of MP (July 2012–July 2014) was 9.04 °C [49]. Relative humidity (RH) of the cave air is

constantly 100%, despite the influence of cold and dry bora winds associated with high pressure, which was recorded by small but abrupt drops of cave air temperature. With the MAAT standard deviation of 0.4 °C (1σ) and constant RH throughout the 2012–2014 period, the MP cave environment may be regarded as stable, and thus favourable for the near-equilibrium precipitation of the spelaean calcite [49]. Discrepancy between the outside and cave MAAT is ascribed to the cave morphology, which, by its descending chambers, acts as a cold trap [61]. Mean annual precipitation of the closest rain gauge station at a similar altitude (Parići village, 3.5 km to the north, 555 m a.s.l.) was 1037 mm for the 1991–2000 period, and shows a bimodal distribution with the maxima during spring and autumn [62]. Precipitation $\delta^{18}O$ indicates influences from both Atlantic and Western Mediterranean vapor masses [63].

3. Materials and Analytical Methods

Two stalagmites, namely MP-2 and MP-3, were collected from below the active dripping sites, both from the niches elevated ca. 2 m from the cave floor. Upon collection, Stalagmate® drip-loggers were installed to record the drip rates, which were, along with the rainfall records, used for the characterization of the karst aquifer. At the same locations, composite monthly water samples were collected for the comparison of the stable isotope composition with meteoric water samples [49]. We also collected two modern calcite samples precipitated on glass plates for the 1/2013–2/2014 period and a third sample from the 2/2014–1/2015 period.

After longitudinal cutting into the halves and polishing, solid pieces of the spelaean carbonate for U-Th dating were extracted using a hand-held dental air drill. The samples were chemically processed and analysed following the methods given in [64,65]. The samples were dissolved in nitric acid and spiked with a mixed ^{229}Th-^{233}U-^{236}U tracer solution. The U and Th were eluted in Eichrom TRU-spec selective ion-exchange resin. Dried samples were then dissolved in diluted nitric acid. Measurements were performed using a Nu Instruments Plasma MC-ICPMS at The University of Melbourne. An initial $^{230}Th/^{232}Th$ ratio was estimated by using the method provided in [66].

For the ^{14}C analyses, solid pieces of MP-3 speleothem were also used to avoid possible contamination with modern atmospheric CO_2 on the outer surface of the samples. Approx. 8–10 mg of each sample was reacted with ~2 mL 85% H_3PO_4 at 90 °C. In the first 5 min of the hydrolysis reaction, CO_2 gas evolved from the outer surface was evacuated from the reaction vessel and not used for ^{14}C analysis. The hydrolysis reaction was maintained at 90 °C for another 1 h. The CO_2 gas derived from the remaining carbonate material was converted to graphite using excess H_2 over an Fe catalyst [67] and the graphite was rear-pressed into an aluminium cathode for accelerator mass spectrometry (AMS) analyses. All stalagmite ^{14}C samples were analysed using the STAR facility at ANSTO [68]. The results were corrected for background and isotopic fractionation using measured $\delta^{13}C$, and normalized to a 95% oxalic acid (HOx-I) standard.

Sampling for stable isotope analysis was done at 1 mm resolution along the growth axis of each stalagmite and along seven growth laminae for the purpose of the Hendy test, using a tungsten carbide dental drill attached to a Taig CNC micromilling lathe. In addition, the isotopic composition of four samples of modern calcite collected on glass plates (1/2013–2/2014 and 2/2014–1/2015) were measured. A total of ca. 600 stable isotope analyses were conducted at The University of Melbourne (Australia) on an AP2003 continuous-flow mass spectrometer. The results are expressed in delta notation with respect to the VPDB standard. Long-term analytical precision of an in-house reference standard (Carrara marble), previously calibrated to international reference materials NBS-18 and NBS-19, was better than 0.05‰ and 0.1‰ (1σ) for $\delta^{13}C$ and $\delta^{18}O$, respectively.

4. Results and Discussion

4.1. Monitoring Background

Results from the monitoring of cave microclimate, characterization of the karst aquifer and hydrological behaviour of the MP-2 and MP-3 drip sites conducted between 7/2012 and 7/2014 have been discussed in [49,63]. In short, while MP-3 showed a fracture flow response to rain events (coefficient of variation (CV) of 140%), MP-2 displayed a more stable drip regime (CV of 59%), very close to the seepage-flow class. Throughout the monitoring period, both sites showed no dripflow interruptions—even during the dry season, the highly responsive MP-3 discharged at ca. 30 drops/hour. Seasonal variations in rainwater stable isotope composition ($\delta^{18}O$ between −9.4‰ and −3.4‰) were attenuated to an amplitude of 0.9‰ for MP-2 and 1.3‰ for MP-3, indicating that the residence time of the infiltrated water in the epikarst is sufficient for homogenization prior to discharge. The discharge is most likely a mixture of slow diffuse (matrix) flow from the overlying beds and fast preferential (fissure) flow [49]. Furthermore, within the relatively stable microclimate conditions in the cave and with well-homogenized dripwater, modern calcite appeared to be deposited close to isotopic equilibrium with the dripwater, when the expression of [69] is applied [49].

4.2. Speleothem Samples

Both speleothems show a relatively inhomogeneous internal structure (Figure 2). The actively growing 15-cm long MP-2 sample consists of two parts formed by the lateral shifting of the drip site (Figure 2). Its interior is marked with clearly visible alterations of different calcite fabrics—from light porous, which becomes laterally narrower in an upwards direction along the growth axis, to dark and compact layers, which drape laterally over the whole speleothem body. A prominent hiatus marked by an eroded layer can be observed at ca. 80 mm from the bottom of the right half of the MP-2 stalagmite.

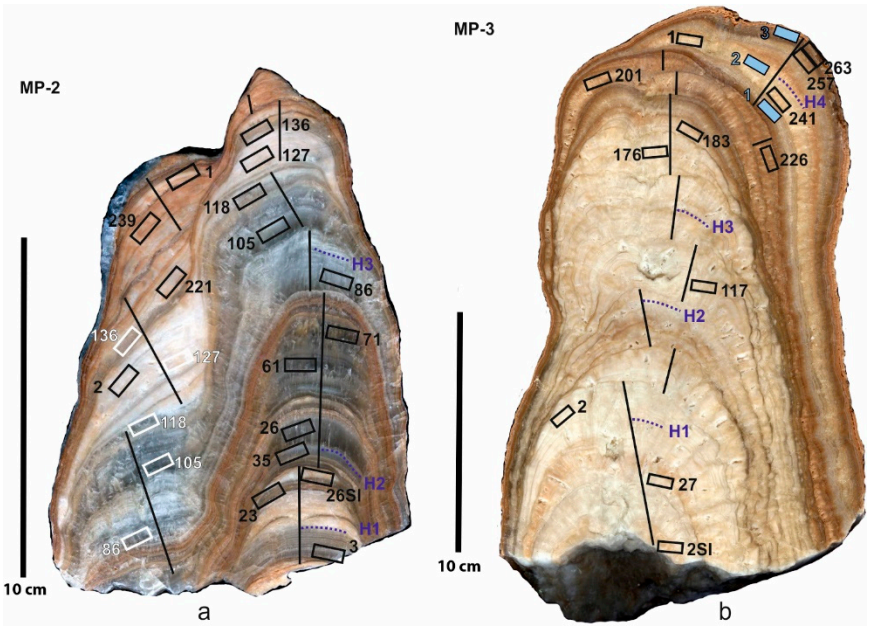

Figure 2. Longitudinal sections of the stalagmites MP-2 and MP-3. Open black squares mark the sample positions for U-Th dating (real depth), open white squares on MP-2 denote the depth positions transposed onto parallel stable isotope tracks and the full light-blue squares mark the ^{14}C-dated samples. Solid lines indicate the growth axes along which the samples for the stable isotopes were taken, and the dotted lines mark the series of samples for the Hendy tests. Note the narrowing of the successive growth layers in the porous white sections and the draping compact darker layers, discussed later in Section 4.4.1.

Stalagmite MP-3 is 25 cm long and also displays a small lateral shift in its growth axis (Figure 2). Prior to collecting, it had been fed by fracture flow, sometimes with a drip intensity of >10,000 drops/hour, and modern calcite has not precipitated, neither on the top of the stalagmite nor on the glass plate installed after removing the speleothem [49]. It seems that, over time, the feeding fracture has widened, enabling transmission of occasionally high discharge and potentially aggressive dripwater, which are unfavourable for calcite deposition.

4.3. Chronology

4.3.1. U-Th Dating and Age–Depth Models

The U-Th dating results are given in Table 1. Uranium concentrations ranged from 17 to 127 ppb with an average value of 63 ppb. At the same time, the $^{230}Th/^{232}Th$ activity ratio was very low and ranged from 1.4 to 22.5, implying a significant contribution of detrital Th in these stalagmites. Consequently, these speleothems proved to be challenging material for U-Th dating. Seven out of 28 age determinations were out of the stratigraphic order (marked with suffix * in the Table 1) and were not included in the age–depth models. Furthermore, five of these age determinations did not yield a meaningful result at all. In the case of the MP-2 speleothem, only one age determination was unsuccessful out of sixteen, while for MP-3 half of the age determinations were rejected (i.e., six out of twelve). Isotopic ratio data of the MP-3 stalagmite point to significant U loss and/or Th gain that is likely a result of post depositional alteration in the upper 70 mm of this stalagmite. We employed the stratigraphic constraint method of [66] to determine the initial $^{230}Th/^{232}Th$ activity ratio of 1.37 ± 0.26 for these speleothems. Corrected ages were calculated by using the U and Th decay constants of [70].

A Monte-Carlo finite positive growth rate model [65,71,72] was employed to construct two independent age–depth models. The first encompasses age data from the upper (younger) portion of the MP-2 stalagmite. During this time period, MP-2 experienced partial contemporaneous growth along two parallel growth axes (Figure 2a). To make use of all U-Th data collected, we transposed the data from the shorter transect to the longer one and ran a unique age–depth model. The five U-Th dates were transposed onto the longer transect based on visual similarity of the two transects and thanks to the pronounced layering of this speleothem. To account for possible extra uncertainty introduced by this procedure, we doubled the original depth uncertainty for all transposed samples and used this value (presented in Table 1) in the age–depth modelling procedure. The positions of the transposed data are indicated with white boxes in Figure 2a and the age–depth model output is presented in Figure 3a.

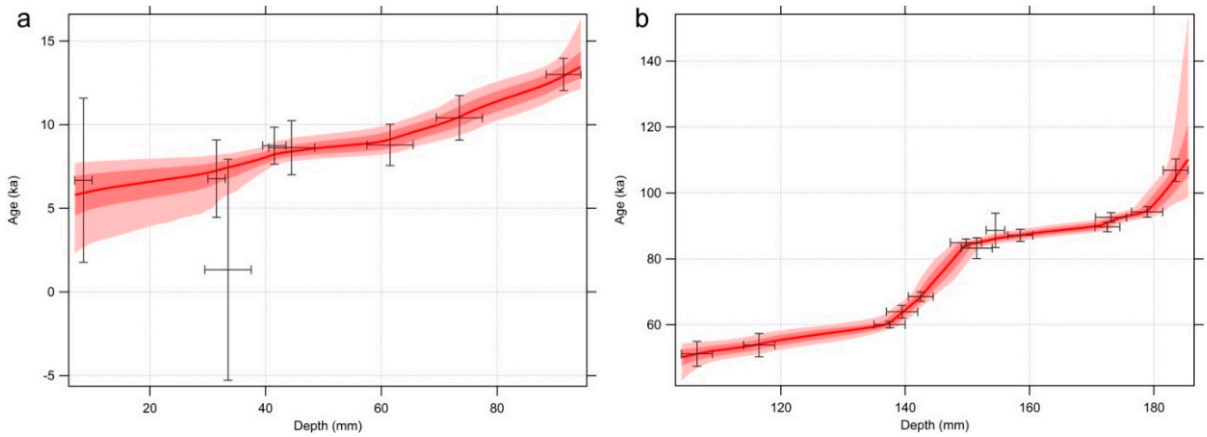

Figure 3. (**a**) Age–depth model for the younger part of MP-2 (from subsample 86 in Figure 2a above); (**b**) composite age–depth model for the older part of the MP-2 (under the subsample 86 in Figure 2a) and MP-3 (from the bottom up to subsample 1 in Figure 2b) stalagmites. Dark red and light red shaded areas represent the 68% and 95% confidence intervals, respectively.

Table 1. U-Th results for the MP-2 and MP-3 stalagmites. Isotopic ratios are the activity ratios and the uncertainties are expressed as 95% confidence intervals (c.i.). Age is corrected for the initial $^{230}Th/^{232}Th$ of 1.37 ± 0.26 following the method of [66]. Results rejected from the age–depth model (outliers) are marked with a suffix *.

Sample Name	Mass (g)	U (ppb)	Depth from Top (mm) (±100% Error)	MP3 on MP2 Depth (mm) (±100% Error Estimated)	$[^{230}Th/^{238}U]$ (±95% c.i.)	$[^{234}U/^{238}U]$ (±95% c.i.)	Uncorrected Age (ky) (±95% c.i.)	$[^{232}Th/^{238}U]$ (±95% c.i.)	$[^{230}Th/^{232}Th]$	Age (ky) (±2 σ unc.)	$[^{234}U/^{238}U]_i$ (±95% c.i.)
MP-2											
MP2-1	0.0770	57	8.5 (1.5)		0.2598 (0.0036)	1.0909 (0.0034)	29.471 (0.451)	0.15122 (0.00325)	1.7	6.677 (4.906)	1.0926 (0.0037)
MP2-239 *	0.1521	127	13.5 (2.0)		0.7608 (0.0038)	0.8804 (0.0027)		0.55274 (0.02425)	1.4		
MP2-221	0.1628	101	31.5 (1.5)		0.1638 (0.0013)	1.0578 (0.0034)	18.266 (0.161)	0.07769 (0.00021)	2.1	6.769 (2.311)	1.0589 (0.0035)
MP2-136	0.1393	67	33.5 (4.0)		0.2671 (0.0021)	1.0600 (0.0036)	31.477 (0.292)	0.18759 (0.00071)	1.4	1.324 (6.608)	1.0602 (0.0038)
MP2-2	0.0720	52	41.5 (2.0)		0.1352 (0.0023)	1.1035 (0.0034)	14.184 (0.254)	0.03957 (0.00041)	3.4	8.746 (1.100)	1.1061 (0.0035)
MP2-127	0.1273	91	44.5 (4.0)		0.1551 (0.0015)	1.0912 (0.0037)	16.633 (0.172)	0.05686 (0.00141)	2.7	8.625 (1.613)	1.0935 (0.0038)
MP2-118	0.2193	44	61.5 (4.0)		0.1410 (0.0021)	1.1001 (0.0036)	14.891 (0.234)	0.04407 (0.00136)	3.2	8.794 (1.238)	1.1026 (0.0037)
MP2-105	0.2194	56	73.5 (4.0)		0.1618 (0.0014)	1.1122 (0.0038)	17.056 (0.159)	0.04848 (0.00129)	3.3	10.410 (1.334)	1.1155 (0.0039)
MP2-86	0.0710	17	91.5 (3.0)		0.1704 (0.0024)	1.1308 (0.0038)	17.706 (0.269)	0.03533 (0.00008)	4.8	13.008 (0.966)	1.1357 (0.0039)
MP2-71	0.1572	38	106.5 (2.5)		0.5148 (0.0043)	1.0919 (0.0034)	68.594 (0.784)	0.12053 (0.00230)	4.3	51.196 (3.737)	1.1062 (0.0040)
MP2-61	0.1546	42	116.5 (2.5)		0.5269 (0.0047)	1.0993 (0.0035)	70.124 (0.859)	0.11444 (0.00210)	4.6	53.833 (3.527)	1.1156 (0.0042)
MP2-26	0.0690	42	137.5 (2.5)		0.5115 (0.0044)	1.1530 (0.0032)	62.792 (0.704)	0.02274 (0.00005)	22.5	60.054 (0.949)	1.1813 (0.0037)
MP2-35	0.0807	99	142.5 (2.5)		0.5433 (0.0046)	1.0916 (0.0036)	73.999 (0.893)	0.04078 (0.00010)	13.3	68.580 (1.456)	1.1112 (0.0043)
MP2-26SI	0.0866	62	151.5 (2.5)		0.6348 (0.0053)	1.0685 (0.0037)	96.767 (1.296)	0.09431 (0.00072)	6.7	83.239 (3.134)	1.0866 (0.0046)
MP2-23	0.0661	97	154.5 (1.5)		0.6882 (0.0037)	1.0617 (0.0044)	111.940 (1.230)	0.15346 (0.00465)	4.5	88.659 (5.237)	1.0793 (0.0056)
MP2-3	0.0930	56	172.5 (2.0)		0.6294 (0.0037)	1.0709 (0.0026)	95.087 (0.903)	0.04027 (0.00065)	15.6	89.698 (1.465)	1.0913 (0.0032)
MP-3											
MP3-263 *	0.1240	37	2.5 (1.5)	125.64 (2.0)	1.3352 (0.0085)	1.0351 (0.0029)		0.55785 (0.00117)	2.4		
MP3-257 *	0.1380	59	8.5 (1.5)	129.6 (2.0)	1.1518 (0.0064)	1.0092 (0.0033)		0.35997 (0.00595)	3.2		
MP3-1	0.0930	30	23.5 (2.0)	139.5 (2.5)	0.5078 (0.0059)	1.0498 (0.0029)	71.423 (1.139)	0.05260 (0.00066)	9.7	63.951 (1.931)	1.0596 (0.0034)
MP3-241 *	0.2135	55	24.5 (2.0)	140.16 (2.5)	0.6120 (0.0040)	1.0397 (0.0030)	95.841 (1.008)	0.10631 (0.00139)	5.8	79.826 (3.531)	1.0497 (0.0037)
MP3-226 *	0.1498	97	36.5 (1.5)	145.26 (2.0)	1.8502 (0.0088)	0.9255 (0.0026)		0.59074 (0.00587)	3.1		
MP3-201 *	0.2330	77	51.5 (1.5)	147.03 (2.0)	1.6433 (0.0072)	0.9453 (0.0028)		0.53569 (0.00378)	3.1		
MP3-183 *	0.1284	80	69.5 (1.5)	149.01 (2.0)	0.7178 (0.0049)	1.0162 (0.0032)	132.579 (1.816)	0.10063 (0.00141)	7.1	117.137 (3.804)	1.0225 (0.0044)
MP3-176	0.2929	77	76.5 (2.0)	149.78 (2.5)	0.5746 (0.0028)	1.0275 (0.0030)	88.667 (0.723)	0.02693 (0.00020)	21.3	84.942 (1.104)	1.0350 (0.0038)
MP3-117	0.0550	49	135.5 (1.5)	158.5 (2.0)	0.6002 (0.0047)	1.0354 (0.0037)	93.629 (1.189)	0.04577 (0.00007)	13.1	87.134 (1.847)	1.0453 (0.0046)
MP3-2	0.0430	42	196.5 (2.0)	173.1 (2.5)	0.6161 (0.0033)	1.0357 (0.0036)	97.552 (0.925)	0.03587 (0.00023)	17.2	92.581 (1.450)	1.0464 (0.0046)
MP3-27	0.2356	68	225.5 (2.0)	178.9 (2.5)	0.6246 (0.0035)	1.0331 (0.0028)	100.205 (0.941)	0.04232 (0.00076)	14.8	94.244 (1.604)	1.0432 (0.0036)
MP3-2SI	0.0730	51	248.5 (1.5)	183.5 (2.5)	0.7009 (0.0065)	1.0421 (0.0023)	120.047 (1.966)	0.08974 (0.00022)	7.8	106.894 (3.425)	1.0569 (0.0031)

The second age–depth model spanned the 110 ka to 45 ka time period, and it is partially presented by both speleothems. In order to produce a single age–depth model, we merged the chronology data from both speleothems. Synchronization was performed following the similar procedure published in [17,73]. In the tuning protocol, the MP-2 dataset was used as the main record because it covered the longer time span compared to the MP-3 speleothem. Eight tie points were selected in MP-3, i.e., the MP-2 $\delta^{18}O$ depth profiles, to transpose $\delta^{18}O$ and $\delta^{13}C$ as well as the corresponding U-Th data of the MP-3 speleothem onto the MP-2 depth scale. Tuning and tie point selection was performed based on visual similarity between the two $\delta^{18}O$ depth series. Linear interpolation was performed in between tie points to transpose all MP-3 data onto the MP2 depth scale. Original depth uncertainty of the MP-3 U-Th samples was increased for at least 25% to account for an extra error introduced by this tuning protocol and this increased uncertainty was then applied in the age–depth modelling procedure. All accepted ages are in stratigraphic order as presented in Figure 3b.

4.3.2. ^{14}C Dating

As pointed out in the previous section, U-Th dating of the uppermost part of the MP-3 speleothem was unsuccessful due to a likely open-system behaviour [74]. Consequently, it was not possible to reliably synchronise this part of MP-3 with MP-2, so those analyses were rejected from the cross-tuning (Figure 3b). To constrain the broad time frame of the youngest deposition phase of MP-3, we employed radiocarbon dating. Its minor role in speleothem geochronology is due to the 'dead (^{14}C-free) carbon' issue [75], where unknown and variable portions of ^{14}C-depleted carbon derive from dissolved old limestone and aged soil-derived carbon. This is expressed as the % dead carbon fraction (DCF) and it varies not only spatially, but also reflects the environmental changes through time [75,76]. An overview of the published speleothem DCF is given in [77] and it ranges from 5% to 37% (with few special cases, such as in Corchia Cave where it is ~60% [76]). Given the measured ^{14}C activities (Table 2), and unknown DCF, we just estimate the youngest portion of the MP-3 speleothem to the MIS-3 period.

Table 2. Conventional ^{14}C ages of the youngest part of the MP-3 speleothem from Manita peć Cave uncorrected for the dead carbon fraction (DCF).

Lab ID	Sample ID	$\delta^{13}C$ (‰ VPDB)	^{14}C Activity (pMC)	Conventional ^{14}C Age (BP)
OZR670	MP3-14C-1	−1.0	0.25 ± 0.03	48,000 ± 1000
OZR671	MP3-14C-2	0.6	0.22 ± 0.02	49,040 ± 660
OZR672	MP3-14C-3	−1.4	0.51 ± 0.03	42,360 ± 410

Measured activity is expressed as pMC (percent modern carbon).

4.4. Stable Isotope Records

Time series of the $\delta^{18}O$ and $\delta^{13}C$ values of the MP-2 and MP-3 speleothems are shown in Figure 4. In MP-2, the $\delta^{18}O$ varies between −5.9‰ and −3.7‰ with an average of −4.8‰, while the $\delta^{13}C$ values are in the range from −7.8‰ to 0.04‰, with an average of −4.9‰. In MP-3, variations in $\delta^{18}O$ are from −5.8‰ to −3.2‰ (average −4.7‰), and $\delta^{13}C$ varies between −7.1‰ and 1.4‰, with an average of −3.6‰. As for MP-3, the $\delta^{18}O$ and $\delta^{13}C$ curves are plotted only for the lower 240 mm (first 242 stable isotope results); that is, from 105.9 ka to 63.7 ka, since the upper part could not be U-Th dated with appropriate certainty. The $\delta^{18}O$ and $\delta^{13}C$ values of the youngest part of MP-3, with roughly estimated ^{14}C ages to MIS-3, vary from −4.9‰ to −4.1‰ and from −1.6‰ to 0.1‰, respectively. Four modern calcite samples collected in the MP cave during the 2/2013–2/2014 and 2/2014–2/2015 periods have an average $\delta^{18}O$ and $\delta^{13}C$ value of −5.4‰ and −10.3‰, respectively.

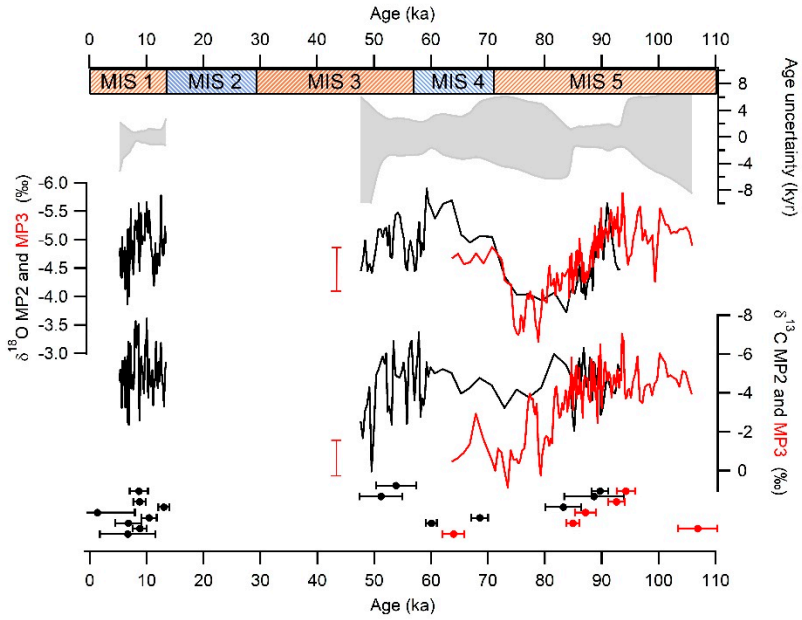

Figure 4. The $\delta^{18}O$ and $\delta^{13}C$ time series of the MP-2 and MP-3 speleothems. Since the chronology of the youngest part of the MP-3 speleothems can be only roughly estimated by ^{14}C dating and cannot be anchored to the particular $\delta^{18}O$ and $\delta^{13}C$ values, their ranges (−4.9 to −4.1‰ and −1.6 to 0.1‰, respectively) are given only by error bars. Bottom: U-Th ages with 2σ uncertainty for MP-2 (black) and MP-3 (red) stalagmites.

Since the credible hydroclimate interpretation of the stable isotope records requires near-equilibrium isotopic fractionation during calcite precipitation from the dripwater [6,43], we employed three different approaches to assess the equilibrium condition. Confirmation of near-equilibrium precipitation during most of the speleothems' growth is given in Appendix A.

4.4.1. Environmental Changes Documented in the $\delta^{13}C$ Signal

$\delta^{13}C$ values along the MP-2 and MP-3 growth axes were within ranges of −7.8 to 0.04‰ and −7.1 to 1.4‰, respectively. Both speleothems recorded significant enrichment in calcite $\delta^{13}C$; ~8.5‰ towards the end of MIS 5 in MP-3, and almost 8.0‰ during MIS 3 in MP-2 (Figure 4), while the lowest $\delta^{13}C$ values, down to −11.1‰, were measured in the modern calcite samples. Such large $\delta^{13}C$ shifts (max. 1.4‰ and min. −11.1‰) in spelaean carbonate usually point to shifts between the C3 and C4 plant communities, where higher values (−6‰ to 2‰) reflect the dominance of C4 plants adapted to arid conditions and lower $\delta^{13}C$ (−14‰ to −6‰) are typical for C3-dominated vegetation [43]. Given the geographical position of MP cave in the temperate zone, and lack of any palynological evidence, we could exclude alteration from a C3 to C4 plant assemblage during the Quaternary climate changes. In the Mediterranean region, the speleothem $\delta^{13}C$ has been used as a proxy for the surface vegetation and soil microbial activity, as revealed in surrounding regions (e.g., [17,20,25–28,30,78–80]). Lower $\delta^{13}C$ values are associated with increased soil pCO_2 produced by intensive soil microbial activity and root respiration during warmer and wetter conditions and/or presence of forest cover, while higher $\delta^{13}C$ values reflect reduced bioproductivity due to enhanced aridity. However, a longer residence time of water within the host rock during the arid periods leads to $\delta^{13}C$ shifting towards higher bedrock-like $\delta^{13}C$ values, and the same effect derives from prior calcite precipitation (PCP), which is again caused by reduced groundwater percolation within the karst aquifer [43,81].

$\delta^{13}C$ variations can be discussed in relation to the speleothem fabrics and growth mode alteration, since the carbonate production, which is controlled by ecological factors and depends on the water chemistry and water supply, determines speleothem geometry [82].

Light porous calcite associated with a retractional growth pattern, i.e., a diameter decrease, was ascribed to reduced hydrologic activity, i.e., dry periods [82–84], while compact layers draping over the stalagmite flanks mark more humid conditions [85]. Such a speleothem architecture is elaborated in the conceptual model in [7], describing the factors influencing stalagmite properties, and is already known from the nearby Modrič Cave [26] as well as from some Spanish [84,86] and Belgian [85] sites. In our MP-2 sample (Figure 2), alteration of calcite fabrics and speleothem geometry are also consistent with $\delta^{13}C$ variations; the white porous parts have high $\delta^{13}C$ values, indicating deprived plant and soil activity in response to enhanced aridity, and are reflected in the narrowing of successive layers, while the darker compact parts, which overlap the preceding layers, coupled with lower $\delta^{13}C$, apparently derive from the wetter phases. In MP-3, the major part of the stalagmite consists of white porous calcite that also gradually narrows towards the top (Figure 2), along with increasing $\delta^{13}C$ values. However, in the subsequent darker layers (in alteration with the lighter ones), $\delta^{13}C$ also remains high. Similarly, in Tana che Urla Cave (central Italy), brown clastic-rich calcite has high isotopic values connected with lower growth rates during drier periods [20]. Apparently, those dark and compact layers derived from phases with limited water availability and decreased soil activity, which might have enhanced soil erosion and induced a higher flux of clastic material in the cave [87]. Evidence of clastic input into MP-3 stalagmite is clearly obvious in the high concentration of detrital thorium (^{232}Th) (Table 1), which prevents precise U-Th dating of the youngest part of MP-3. We presume that part was formed during phases of climatic deterioration within MIS 3, when reduced rainfall increased the residence time of percolating groundwater within the host rock, resulting in enriched $\delta^{13}C$ due to the heavier carbon isotopic composition of the limestone [88]. The dominance of the bedrock isotopic composition (higher $\delta^{13}C$), i.e., lack of $\delta^{13}C$-lighter soil-derived organic carbon in the system, is best pronounced in LGM-speleothems formed underneath an ice cover [35] or presently in near-freezing conditions [89], where the carbonic acid dissolution (CAD) has been replaced by the sulphuric acid dissolution (SAD) [76] throughout periods when conditions are unfavourable for the production of pedogenic CO_2. However, in accordance with the local sulphur-free lithology (Upper Jurassic limestone), this consistently high $\delta^{13}C$ values of the youngest part of MP-3, roughly dated at mid-MIS 3, are presumably the result of CAD, which took place in an environment with minimal but apparently sufficient biological activity. Namely, glacial periods left some landmarks in the surroundings of MP, such as LGM terminal moraine in Rujanska kosa (6 km NW from MP cave) at the present altitude of 920 m a.s.l. [90], and tills reaching a minimum altitude of 800 m a.s.l. [91]. Given the fact that the recharge area and the source of pedogenic CO_2 that reaches MP cave is mostly at the altitude of ca. 700 m a.s.l., this was the glacier-free area, but most likely the periglacial setting maintained low plant and soil bioactivity levels. Hence, the lack of $\delta^{13}C$-lighter soil-derived organic carbon, and the apparent aridity that could sustain PCP and prolong the interaction between the percolating groundwater and the host rock, resulted in an overall $\delta^{13}C$ increase.

As our time constraint based on ^{14}C dating is not completely confident, the MIS 3 record from adjacent Modrič Cave (9 km SE from MP) might confirm our findings; namely, that stalagmite MOD-21 deposited from 54.6 ka to 44.0 ka recorded the same increasing trend within the $\delta^{13}C$ range of 8‰, associated with a dry phase, and followed by a non-depositional period [26]. Likewise, growth of MP-3, after the cessation within MIS-3, was not restored.

The other extreme, the lowermost $\delta^{13}C$ values within the MP cave, were recorded in modern samples (from −11.1‰ to −9.2‰), although the terrain above the cave, in fact the whole recharge area, is presently almost bare bedrock with scarce bush patches (Figure 1b). Such a landscape is the result of anthropogenic and natural processes that led to deforestation due to the overuse of the Velebit Mountain woodlands during the 16th–17th c. by the invaders (Venetians, Otomans and Habsburgs) [92] and growing local population. The Little Ice Age also reinforced forest logging. In spite of reforestation, organized already in the late 19th century [93] and naturally intensified upon the ban of goat breeding in

1950s, the recovery of the woodland has been slow, if happening at all. At the moment, it seems unrealistic that such negative $\delta^{13}C$ values of modern calcite can be produced by such modest pedologic and vegetation cover; however, this has been repeatedly confirmed. Similarly, a low modern calcite $\delta^{13}C$ has been measured in adjacent Modrič Cave (32 m a.s.l; 9 km SE from MP) and Strašna peć Cave (74 m a.s.l; 48 km SW from MP). In modern calcite precipitated during 1999–2007 in Modrič Cave, $\delta^{13}C$ was −8.2‰ and −9.8‰ [48], while in Strašna peć Cave, calcite deposited through 2013–2014 had values from −12.1‰ to −8.7‰ (mean −10.8‰, n = 8) ([49] and unpublished data). Both sites are also characterized by patches of soil with sparse Mediterranean maquis, slightly more developed than the above MP Cave, which apparently gives enough biological activity to sustain such low $\delta^{13}C$ values.

4.4.2. Hydroclimate Variations from MIS 5 to MIS 3 as Recorded by Spelean $\delta^{18}O$

In contrast to $\delta^{13}C$, variations in $\delta^{18}O$ in MP-2 and MP-3 are much smaller, with similar ranges of −5.9 to −3.7‰ and −5.8 to −3.2‰, respectively. Although not of the highest resolution and precision, their pattern is comparable to the millennial-scale climate variability in Greenland [2] (Figure 5), which has already been recognized in other speleothem records in the Mediterranean realm, e.g., [12,24,25], in the southern Alps [23] and the north Alpine speleothem records [4,36–39].

As already mentioned, the precipitation amount is a dominant factor controlling speleothem $\delta^{18}O$ in the Mediterranean (e.g., [9–18,20–33]); but, as the source of the moisture can also vary with time [25,94,95], both the amount and source effects must be taken into consideration. Contemporary spatio-temporal variations in Atlantic and Mediterranean vapour-source influences on Eastern Adriatic coast are discussed in [49,63,96–99].

The $\delta^{18}O$ record from the MP cave starts at GS 24, which is, unlike in our record, very well expressed by a positive shift in other regional records, such as from Croatian Mljet Island (MSM) [27], Corchia Cave in the Apuan Alps [100], Apulian Pozzo Cucú Cave (PC) [25], Israeli Soreq and Peqiin caves [33], but also in North Alpine stalagmites (NALPS) [4] and Western Mediterranean marine core GDEC-4-2 [58] (Figure 5). It was obviously an event of broad regional significance characterized by cooling of the SW and S Europe due to the renewed Northern Hemisphere ice-sheet growth after the end of the last interglacial, and a reduction in atmospheric moisture [100]. During the next 15 ka, which in NGRIP is documented by gradual climate deterioration from GI 23 throughout the relatively long GS 23, our MP-3 recorded several $\delta^{18}O$ excursions, similar to the PC record [25]. Since this part of MP history is supported only by a single speleothem, we refrain from drawing any specific conclusions except that the MP-3 speleothem architecture and fabrics suggest arid conditions.

The following period, from MIS 5c to MIS 4, is instead covered by both MP stalagmites, complemented by the earlier findings from submerged speleothems [101]; namely, one of the consequences of global climate changes is sea-level changes caused by the accumulation and melting of continental ice. In the shallow northern part of the Adriatic Sea, this generated substantial palaeogeography changes throughout the Quaternary due to shifting coastlines (Figure 6c) and exposing of the carbonate landscape to karstification, including speleothem precipitation. Two such speleothems are K-14 and K-18 from submerged U Vode Pit near Krk Island (96 km NW from MP), whose deposition was repeatedly interrupted by the MIS 5 sea-level fluctuations [101] (Figure 6a,b).

The oldest part of K-18 precipitated from >93 to 90 ka in a similarly narrowing manner as the MP samples by the end of cool and dry GS 23 (Figure 5). The subsequent GS 22 was even more pronounced as recorded by the $\delta^{18}O$ increase in MP speleothems and those from Mljet Island, Apulia and Sardinia, and the most prominent decrease in the NALPS record. It was associated with the MIS 5b sea-level fall, enabling K-18 deposition from 90 to 87 ka. Its porous white calcite (Figure 6a) resembles that of MP-3, pointing to the similar environmental setting. An abrupt shift in $\delta^{18}O$ towards more negative values in Mediterranean speleothems (and towards positive in NALPS) marks the beginning of GI

21 and the MIS 5a sea-level highstand that flooded U Vode Pit and temporarily ceased K-14 and K-18 growth. Towards the MIS 4 glacial, increasing speleothem $\delta^{18}O$ suggest progressive climate deterioration (cooling and drying) and resulting sea-level fall during which K-18 reactivated. Its dark and compact calcite precipitated from 82 ka to 77 ka—the short period presumably related to the mild stadial of GS 20, which is, along with GS 21, GI 20 and GI 19, relatively well expressed in the MP-3 record.

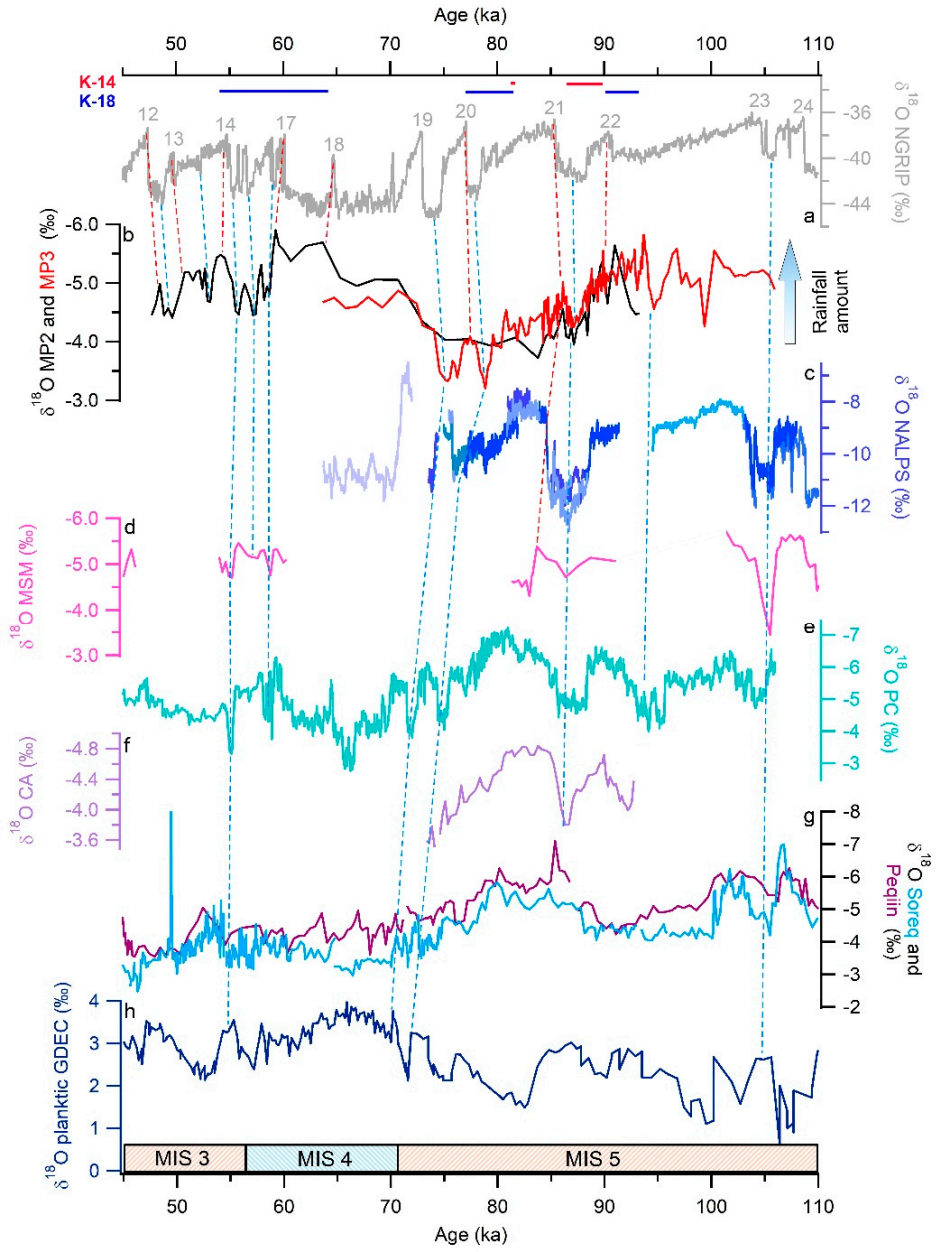

Figure 5. Comparison of $\delta^{18}O$ records from (**a**) the NGRIP ice core $\delta^{18}O$ record [2]; (**b**) Manita peć Cave stalagmites MP-2 and MP-3; (**c**) NALPS record from the North Alps caves [4]; (**d**) Mala Špilja Cave from Mjet Island [27]; (**e**) Pozzo Cucú Cave [25]; (**f**) Crovassa Azzurra Cave [24]; (**g**) Soreq and Peqiin caves in Israel [33]; and (**h**) marine borehole GDEC-4-2 [59]. Numbers refer to Greenland Interstadials. Dashed lines indicate the most prominent matches of recorded stadials (blue) and interstadials (red). Horizontal bars represent growth episodes of speleothems K-14 (red) and K-18 (blue) recovered from the submerged U Vode Pit (Krk Island) [101].

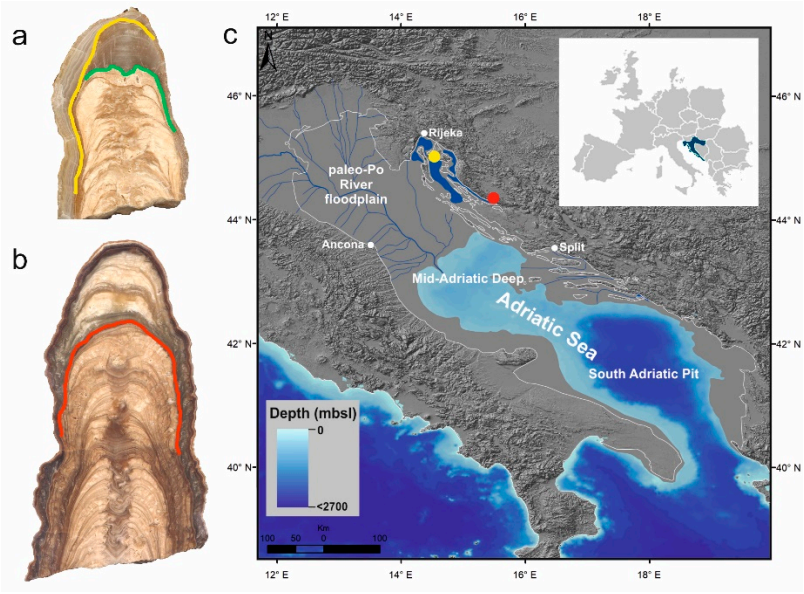

Figure 6. Longitudinal section of submerged speleothems (**a**) K-18 and (**b**) K-14 from U Vode Pit (Krk Island) with marked hiatuses caused by sea transgression [101] during 77–64 ka (yellow), 90–82 ka (green) and 87–82 ka (red). (**c**) Palaeogeography of the study area during the LGM (modified after [54], with the present coastline given in white. Note the distance of the MP cave (red dot) and Krk Island area (yellow dot) from the then coastline. (Reprinted from Paleogeography, Palaeoclimatology, Palaeoecology, 544, Brunović, D., Miko, S., Hasan, O., Papatheodorou, G., Ilijanić, N., Miserocchi, S., Correggiari, A., Geraga, M.: Late Pleistocene and Holocene paleoenvironmental reconstruction of a drowned karst isolation basin (Lošinj Channel, NE Adriatic Sea), 109587, Copyright (2020), with permission from Elsevier.)

The most pronounced temperature drop during the studied period occurred in MIS 4, at least as far as the Greenland temperature is concerned (Figure 5). At its peak (~65 ka), with an ~80 m lower sea level [102], the coastline of the NE Adriatic nearest to the MP cave receded ~70 km away from the present position (3.7 km from the coast). Environmental conditions certainly changed and climate type most probably altered to Df (humid continental), which today dominates the highest peaks of the Velebit Mountain [49]. Nevertheless, the $\delta^{18}O$ in both the MP-2 and MP-3 speleothems remains relatively low. It is apparent that the glacial climate in the eastern Adriatic, as recently shown on the western coast of Apulia [25], was milder and sufficiently moist for speleothem deposition. The growth episode of speleothem K-18 between 64 ka and 54 ka (Figure 5) confirms this [101].

The end of MIS 5 was a period of decoupled MP $\delta^{13}C$ and $\delta^{18}O$ series, with a general rise in $\delta^{18}O$, and not so much increased or stable $\delta^{13}C$ (Figure 4). Such a situation is regionally interpreted as a time of prevailing source effect over amount effect [24,25], which is attributed to the less efficient Atlantic Meridional overturning circulation during ice-sheet growth [18,103]; namely, with lower production of Atlantic moisture and changed westerlies trajectories, the relative proportion of Atlantic (more negative $\delta^{18}O$) and Mediterranean (less negative $\delta^{18}O$) moisture changes, and the region receives isotopically enriched precipitation. The opposite situation, i.e., covarying $\delta^{13}C$ and $\delta^{18}O$, is ascribed to periods of similar climate control [24]; that is, the amount of precipitation that governs vegetation growth and soil bioactivity. Our record only partially follows this scheme. One of the possible causes of that discrepancy might derive from a reorganized geographical setting, since the MP site with a lowered sea level became a region with more pronounced orographic precipitation instead (or in spite) of enhanced aridity.

According to the $\delta^{18}O$ variations in MP-2, the transition from MIS 4 to MIS 3 is characterized by short and rapid oscillations matching GI 17 to GS 13. It was also a depositional period of the MSM-1 stalagmite from Mljet Island and K-18 from Krk Island,

both of which, however, stopped growing after the dry and cold stadial GS 15, the one also very prominent in Apulia [25] and SE Spain [12]. The same period in MP cave is marked with oscillating and finally increasing $\delta^{13}C$, leading to the highest $\delta^{13}C$ values and therefore quite arid conditions. Meanwhile, in the Apulian karst, a soil bioproductivity plateau was reached ($\delta^{13}C$ = ~−8‰) despite the gradual $\delta^{18}O$ increase; i.e., a precipitation decrease [25].

4.4.3. MIS 2 to MIS 1 Transition in $\delta^{18}O$ Record

The transition from MIS 2 to MIS 1 is captured in the youngest part of the MP-2 stalagmite. According to the age–depth model, deposition of the youngest part of MP-2 recommenced around 13.8 ka (Figure 7), and our last time series data is at 5.3 ka (actively growing topmost part was not dated). The $\delta^{18}O$ values are in range between −5.8‰ and −3.9‰ (average −4.9‰). The lowest $\delta^{18}O$ value implies relatively warm and humid conditions at 12.57 $^{+1.11}/_{-1.08}$ ka, followed by abrupt climate deterioration and high isotopic values at 11.33 $^{+1.15}/_{-1.10}$ ka, which may, within the corresponding age uncertainties, correspond to the cool and dry Younger Dryas event (12.9–11.7 ka). However, the apparent delay from the $\delta^{18}O$ excursion recorded in, e.g., the Corchia [15] and Soreq Cave speleothems [33], as well as in the NGRIP core [2], should be checked in other contemporaneous speleothems or other archives, rather than be prematurely ascribed to specific local conditions.

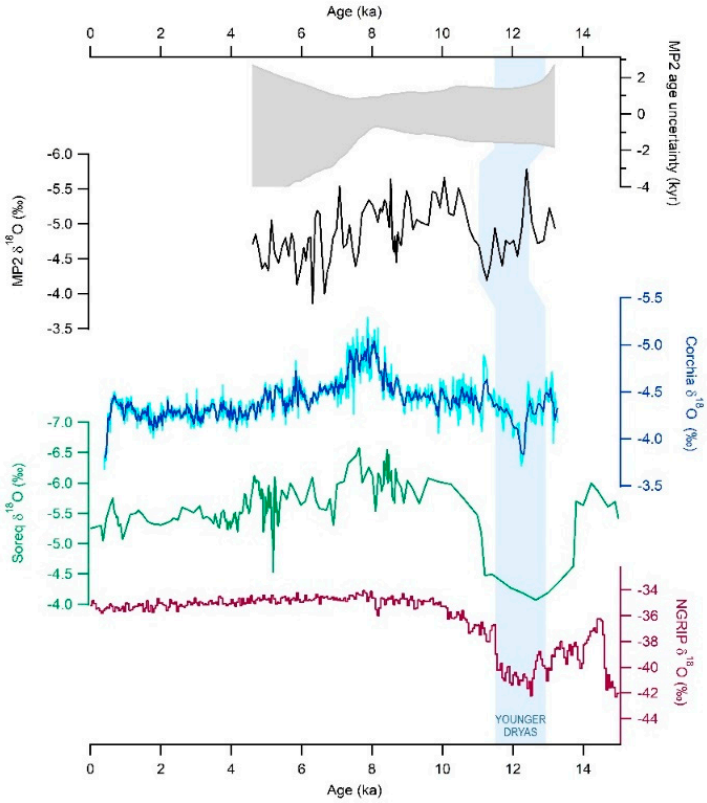

Figure 7. Comparison of the $\delta^{18}O$ variation in the younger part of the MP-2 speleothem with other contemporaneous $\delta^{18}O$ speleothem records from the Corchia [15] and Soreq caves [33] and with NGRIP $\delta^{18}O$ data [2], with the prominent excursion ascribed to the Younger Dryas climatic event.

5. Conclusions

Manita peć Cave preserves speleothem records of environmental conditions over the last glacial cycle at a very specific location—the littoral part of the northern Mediterranean (eastern Adriatic coast), but at an elevation close to the glaciation limit during the glacial phases. The main features of the changing environment obtained from the $\delta^{18}O$ and $\delta^{13}C$ records from two partially coeval speleothems can be summarized as follows:

- Millennial scale climate events, i.e., Dansgaard–Oeschger (DO) cycles, reconstructed from $\delta^{18}O$ variations were superimposed upon longer-lasting climate fluctuations, and within the MIS 5–MIS 3 period the $\delta^{18}O$ variations were synchronous with GI-GS 22, GI-GS 21, GI-GS 20, GI 19 and from GI-GS 17 to GI-GS 13. Most of these shifts, related to the change in precipitation amount, are consistent with speleothem records from the Adriatic and western Mediterranean regions.
- The presumed Younger Dryas $\delta^{18}O$ signal requires confirmation by a coeval MP speleothem or other local proxy records.
- $\delta^{13}C$, as a proxy for the vegetation status and microbial activity in the soil, showed increasing values on longer time scales, pointing to general drying trend towards MIS 3 and MIS 4. With a positive shift of ~8‰, $\delta^{13}C$ approached the values of the host rock due to the long residence time of the groundwater within epikarst fractures and probable enhanced prior calcite precipitation—both a consequence of intensive aridity. According to geomorphic studies, the MP area was glacier-free, and carbonic acid dissolution was the driving force of the karstification processes throughout all deposition periods, no matter how modest the vegetation was.
- The MP results complement findings from adjacent submerged speleothems: parts of the samples from both sites consist of white porous calcite, with a narrowing trend from the colder and drier periods and glacial/stadial sea-level lowstands. Warmer and wetter conditions and consequent sea-levels highstands are marked with hiatuses within the submerged speleothems and compact calcite draping over the narrow cold-phase stalagmite bodies.
- In terms of palaeogeography, the recorded climate changes played a key role in land-sea distribution, transforming the near-coastal site of MP into a continental one during the glacial/stadial stages. We assume that such settings during the MIS 4 attenuated aridity of the glacial period by promoting the MP cave into a site receiving somewhat higher amounts of orographic precipitation.
- Accordingly, we also assume that switching the predominance between the amount and source effect, which was proven regionally, might be overprinted by local site-specific features, such as in the MP site.

Author Contributions: Conceptualization, M.S., R.L. and N.L.; methodology, M.S., R.N.D., P.B., J.C.H. and Q.H.; investigation, M.S., R.L., N.L. and P.B.; resources, M.S., R.N.D. and J.C.H.; writing—original draft preparation, M.S., P.B. and R.L.; writing—review and editing, M.S., R.N.D., P.B., R.L., N.L. and Q.H.; visualization, M.S. and P.B.; funding acquisition, M.S. All authors have read and agreed to the published version of the manuscript.

Funding: This research was funded by the University of Zadar (Scientific Project 60200 Reconstruction of the regional palaeoclimate change—speleothem records from the North Dalmatia (Croatia).

Institutional Review Board Statement: Not applicable.

Informed Consent Statement: Not applicable.

Data Availability Statement: Stable and U-series isotope data are archived in the SISAL database and will be freely available by the next update (SISAL_v3).

Acknowledgments: The management and the stuff of the National Park Paklenica are gratefully acknowledged for the cooperation and logistic support, and Nenad Buzjak for the field assistance. We thank Dea Brunović for providing the background for Figure 6c. Two anonymous reviewers are acknowledged for their constructive suggestions.

Conflicts of Interest: The authors declare no conflict of interest. The funders had no role in the design of the study; in the collection, analyses, or interpretation of data; in the writing of the manuscript, or in the decision to publish the results.

Appendix A

Isotopic Equilibrium

A prerequisite for credible interpretation of palaeoenvironmental changes from $\delta^{18}O$ and $\delta^{13}C$ records is near-equilibrium isotopic fractionation during calcite precipitation from the dripwater [6,43]. To assess this, we used three conventional approaches: the Hendy test [6], replication test [104] and a comparison of the measured cave air temperature with that calculated from the modern calcite, according to empirical relationships for water–calcite oxygen isotope fractionation [69]; namely, according to [105], if the modern calcite equilibrium conditions can be confirmed, then we can assume that ancient speleothems from the same cave should also have been precipitated at or near isotopic equilibrium.

Graphical presentations of the Hendy tests performed along three growth laminae on MP-2 and four laminae on MP-3 stalagmite are given on Figures A1 and A2. The first Hendy criterion of the $\delta^{18}O$ values remaining constant along a single growth layer in support of equilibrium deposition [6] was fulfilled in all cases since the maximal $\delta^{18}O$ variations were 0.53‰ and 0.49‰ within the MP-2 and MP-3 layers, respectively (Figure A1), both below the threshold value of 0.8‰ defined by [106]. The only slight enrichment in calcite $\delta^{18}O$ with distance from the growth axis was observed in the MP-3 H3 series. The second criterion of no correlation between the $\delta^{18}O$ and $\delta^{13}C$ values along a single lamina [6] was also satisfied (Figure A2), with the exception of laminae H1 in MP-2 and H3 in MP-3, which returned Pearson's correlation coefficients of r = 0.80 and r = 0.83, respectively, while their p-value describing the statistical significance of the correlations were $p < 0.05$, pointing to significant correlations. However, possible covariation in certain growth phases is not exclusively proof of kinetic fractionation, since both $\delta^{18}O$ and $\delta^{13}C$ can be controlled by climate (via hydrological response and plant/soil activity) and thus might covary [104].

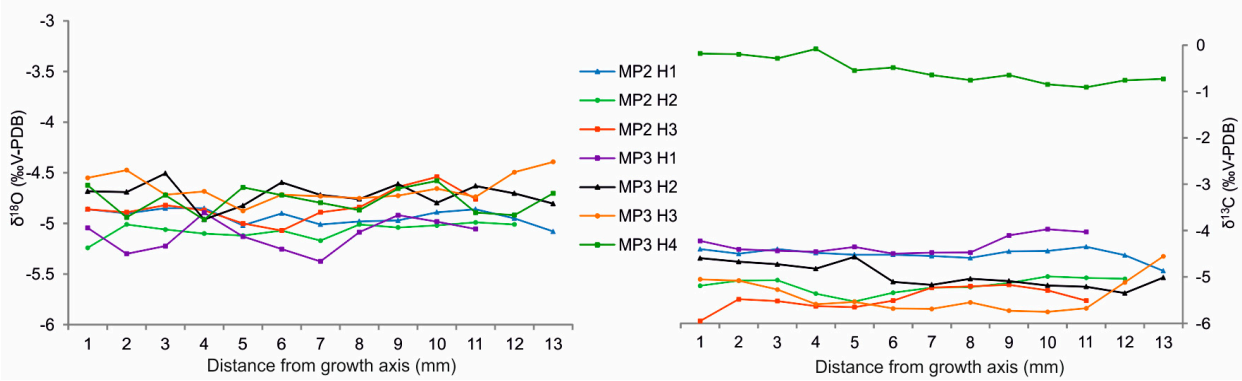

Figure A1. $\delta^{18}O$ and $\delta^{13}C$ values along the MP-2 and MP-3 growth layers selected for the Hendy tests [6]. For the location of the sampling tracks, see Figure 2. Equilibrium deposition is presumed due to the lack of a significant trend in the isotopic ratios towards heavier isotopic values away from the growth axis.

Since the Hendy test is not considered as explicit proof, the replication test is more reliable [104] and was used to additionally support the independence of isotopic composition on kinetic processes; namely, similarity of the isotopic profiles could have occurred either because the kinetic and/or vadose zone processes affected both speleothems equally (which is hardly possible) or, more likely, it was absent [104]. As the resemblance of $\delta^{18}O$ shifts between an older part of MP-2 and MP-3 is evident (Figure A1), we can assume that, at least during that period, precipitation of calcite was close to isotopic equilibrium with cave water, and spelaean $\delta^{18}O$ was controlled exclusively by the cave temperature and water $\delta^{18}O$, in response to palaeoenvironmental changes above the MP cave.

Knowing the oxygen values of the modern calcite ($\delta^{18}O_C$) and dripwater ($\delta^{18}O_W$), an additional proof of near-equilibrium condition can be provided based on the matching of the measured cave air temperature (T_m) with the one calculated (T_c) after the empirical relationships for water–calcite oxygen isotope fractionation given by the equation $1000 \ln \alpha = 16.1(10^3\ T^{-1}) - 24.6$ [69], where $\alpha = (1000 + \delta^{18}O_C)/(1000 + \delta^{18}O_W)$. As established

earlier in [49] using four modern MP calcite samples, the T_c range from 9.1 ± 0.1 °C to 10.4 ± 0.1 °C matches well the T_m = 9.04 °C, giving further confidence in the isotopic record as a reliable source for palaeoenvironmental reconstruction.

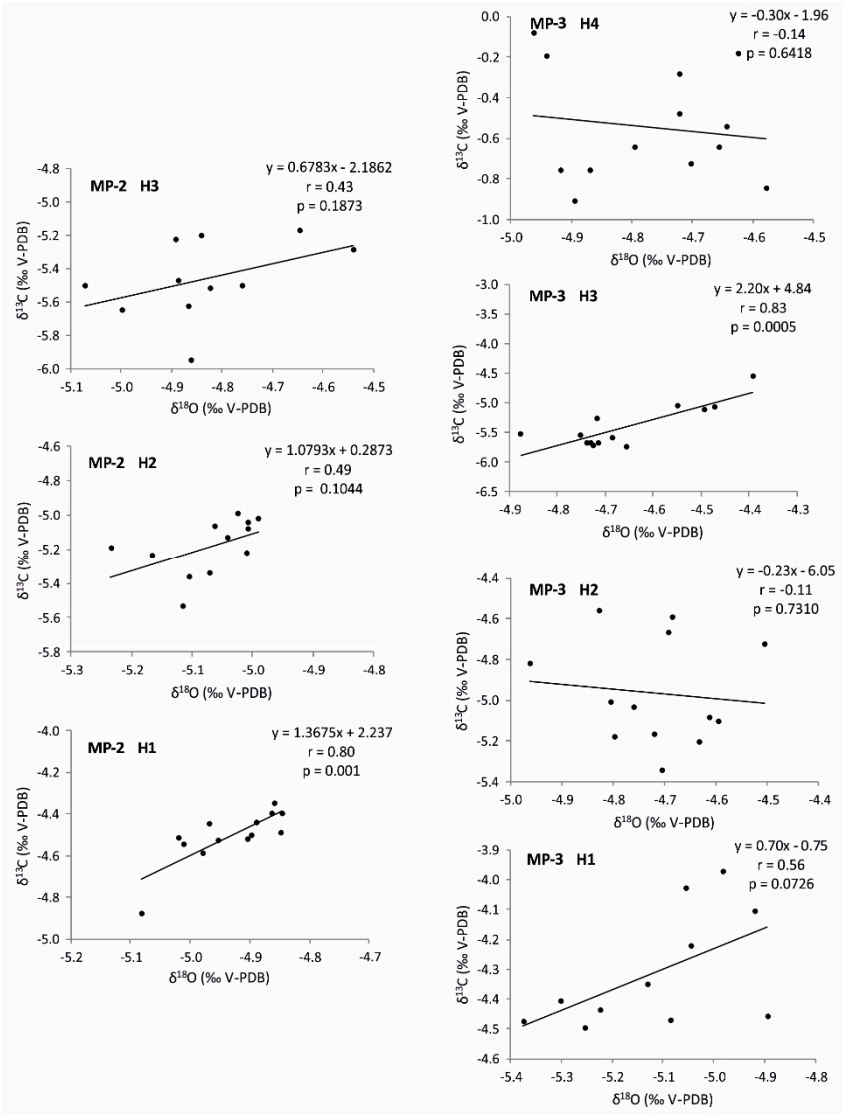

Figure A2. Plots of $\delta^{18}O$–$\delta^{13}C$ pairs from single growth layers in MP-2 (left column) and MP-3 (right column) stalagmites. For the location of the sampling tracks, see Figure 2.

References

1. Dansgaard, W.; Johnsen, S.J.; Clausen, H.B.; Dahl-Jensen, D.; Gundestrup, N.S.; Hammer, C.U.; Hvidberg, C.S.; Steffensen, J.P.; Sveinbjörnsdottir, A.E.; Jouzel, J.; et al. Evidence for general instability of past climate from a 250-kyr ice-core record. *Nature* **1993**, *364*, 218–220. [CrossRef]
2. North GRIP Members. High-resolution record of Northern Hemisphere climate extending into the last interglacial period. *Nature* **2004**, *431*, 147–151. [CrossRef] [PubMed]
3. Rousseau, D.-D.; Kukla, G.; McManus, J. What is what in the ice and the ocean? *Quat. Sci. Rev.* **2006**, *25*, 2025–2030. [CrossRef]
4. Moseley, G.E.; Spötl, C.; Brandstätter, S.; Erhardt, T.; Luetscher, M.; Edwards, R.L. NALPS19: Sub-orbital-scale climate variability recorded in northern Alpine speleothems during the last glacial period. *Clim. Past* **2020**, *16*, 29–50. [CrossRef]
5. Corrick, E.C.; Drysdale, R.N.; Hellstrom, J.C.; Capron, E.; Rasmussen, S.O.; Zhang, X.; Fleitmann, D.; Couchoud, I.; Wolff, E. Synchronous timing of abrupt climate changes during the last glacial period. *Science* **2020**, *369*, 963–969. [CrossRef] [PubMed]
6. Hendy, C.H. The Isotopic Geochemistry of Speleothems—I. The Calculation of the Effects of Different Modes of Formation on the Isotopic Composition of Speleothems and Their Applicability as Palaeoclimatic Indicators. *Geochim. Cosmochim. Acta* **1971**, *35*, 801–824. [CrossRef]
7. Fairchild, I.J.; Baker, A. *Speleothem Science: From Process to Past Environments*; Wiley-Blackwell: Chichester, UK, 2012.

8. Rozanski, K.; Araguás-Araguás, L.; Gonfiantini, R. Isotopic patterns in modern global precipitation. *Clim. Chang. Cont. Isot. Rec.* **1993**, *78*, 1–36. [CrossRef]
9. Moreno, A.; Pérez-Mejías, C.; Bartolomé, M.; Sancho, C.; Cacho, I.; Stoll, H.; Delgado-Huertas, A.; Hellstrom, J.; Edwards, R.L.; Cheng, H. New speleothem data from Molinos and Ejulve caves reveal Holocene hydrological variability in northeast Iberia. *Quat. Res.* **2017**, *88*, 223–233. [CrossRef]
10. Rossi, C.; Bajo, P.; Lozano, R.P.; Hellstrom, J. Younger Dryas to Early Holocene paleoclimate in Cantabria (N Spain): Constraints from speleothem Mg, annual fluorescence banding and stable isotope records. *Quat. Sci. Rev.* **2018**, *192*, 71–85. [CrossRef]
11. Baldini, L.M.; Baldini, J.U.L.; McDermott, F.; Arias, P.; Cueto, M.; Fairchild, I.J.; Hoffmann, D.; Mattey, D.P.; Müller, W.; Nita, D.C.; et al. North Iberian temperature and rainfall seasonality over the Younger Dryas and Holocene. *Quat. Sci. Rev.* **2019**, *226*, 105998. [CrossRef]
12. Budsky, A.; Scholz, D.; Wassenburg, J.A.; Mertz-Kraus, R.; Spötl, C.; Riechelmann, D.F.; Gibert, L.; Jochum, K.P.; Andreae, M.O. Speleothem $\delta^{13}C$ record suggests enhanced spring/summer drought in south-eastern Spain between 9.7 and 7.8 ka—A circum-Western Mediterranean anomaly? *Holocene* **2019**, *29*, 1113–1133. [CrossRef]
13. Denniston, R.F.; Houts, A.N.; Asmerom, Y.; Wanamaker, A.D., Jr.; Haws, J.A.; Polyak, V.J.; Thatcher, D.L.; Altan-Ochir, S.; Borowske, A.C.; Breitenbach, S.F.M.; et al. A stalagmite test of North Atlantic SST and Iberian hydroclimate linkages over the last two glacial cycles. *Clim. Past* **2018**, *14*, 1893–1913. [CrossRef]
14. Thatcher, D.L.; Wanamaker, A.D.; Denniston, R.F.; Asmerom, Y.; Polyak, V.J.; Fullick, D.; Ummenhofer, C.C.; Gillikin, D.P.; Haws, J.A. Hydroclimate variability from western Iberia (Portugal) during the Holocene: Insights from a composite stalagmite isotope record. *Holocene* **2020**, *30*, 966–981. [CrossRef]
15. Zanchetta, G.; Drysdale, R.N.; Hellstrom, J.C.; Fallick, A.E.; Isola, I.; Gagan, M.K.; Pareschi, M.T. Enhanced rainfall in the Western Mediterranean during deposition of sapropel S1: Stalagmite evidence from Corchia cave (Central Italy). *Quat. Sci. Rev.* **2007**, *26*, 279–286. [CrossRef]
16. Zanchetta, G.; Bar-Matthews, M.; Drysdale, R.N.; Lionello, P.; Ayalon, A.; Hellstrom, J.C.; Isola, I.; Regattieri, E. Coeval dry events in the central and eastern Mediterranean basin at 52 and 56 ka recorded in Corchia (Italy) and Soreq caves (Israel) speleothems. *Glob. Planet. Chang.* **2014**, *122*, 130–139. [CrossRef]
17. Drysdale, R.N.; Zanchetta, G.; Hellstrom, J.C.; Fallick, A.E.; Zhao, J.-X.; Isola, I.; Bruschi, G. Palaeoclimatic implications of the growth history and stable isotope ($\delta^{18}O$ and $\delta^{13}C$) geochemistry of a Middle to Late Pleistocene stalagmite from central-western Italy. *Earth Planet. Sci. Lett.* **2004**, *227*, 215–229. [CrossRef]
18. Drysdale, R.N.; Hellstrom, J.C.; Zanchetta, G.; Fallick, A.E.; Goñi, M.F.S.; Couchoud, I.; McDonald, J.; Maas, R.; Lohmann, G.; Isola, I. Evidence for obliquity forcing of glacial termination II. *Science* **2009**, *325*, 1527–1531. [CrossRef]
19. Zhornyak, L.V.; Zanchetta, G.; Drysdale, R.N.; Hellstrom, J.; Isola, I.; Regattieri, E.; Piccini, L.; Baneschi, I.; Couchoud, I. Stratigraphic evidence for a "pluvial phase" between ca. 8200–7100 ka from Renella Cave (Central Italy). *Quat. Sci. Rev.* **2011**, *30*, 409–417. [CrossRef]
20. Regattieri, E.; Zanchetta, G.; Drysdale, R.N.; Isola, I.; Hellstrom, J.C.; Roncioni, A. A continuous stable isotope record from the penultimate glacial maximum to the Last Interglacial (159-121 ka) from Tana Che Urla Cave (Apuan Alps, central Italy). *Quat. Res.* **2014**, *82*, 450–461. [CrossRef]
21. Regattieri, E.; Zanchetta, G.; Drysdale, R.N.; Isola, I.; Hellstrom, J.C.; Dallai, L. Lateglacial to Holocene trace element record (Ba, Mg, Sr) from Corchia Cave (Apuan Alps, central Italy): Paleoenvironmental implications. *J. Quat. Sci.* **2014**, *29*, 381–392. [CrossRef]
22. Columbu, A.; Drysdale, R.; Capron, E.; Woodhead, J.; De Waele, J.; Sanna, L.; Hellstrom, J.; Bajo, P. Early last glacial intra-interstadial climate variability recorded in a Sardinian speleothem. *Quat. Sci. Rev.* **2017**, *169*, 391–397. [CrossRef]
23. Columbu, A.; Sauro, F.; Lundberg, J.; Drysdale, R.; De Waele, J. Palaeoenvironmental changes recorded by speleothems of the southern Alps (Piani Eterni, Belluno, Italy) during four interglacial to glacial climate transitions. *Quat. Sci. Rev.* **2018**, *197*, 319–335. [CrossRef]
24. Columbu, A.; Spötl, C.; De Waele, J.; Yu, T.-L.; Shen, C.-C.; Gázquez, F. A long record of MIS 7 and MIS 5 climate and environment from a western Mediterranean speleothem (SW Sardinia, Italy). *Quat. Sci. Rev.* **2019**, *220*, 230–243. [CrossRef]
25. Columbu, A.; Chiarini, V.; Spötl, C.; Benazzi, S.; Hellstrom, J.; Cheng, H.; De Waele, J. Speleothem record attests to stable environmental conditions during Neanderthal—Modern Human turnover in Southern Italy. *Nat. Ecol. Evol.* **2020**, *4*, 1188–1195. [CrossRef] [PubMed]
26. Rudzka, D.; Mcdermott, F.; Surić, M. A Late Holocene Climate Record in Stalagmites from Modrič Cave (Croatia). *J. Quat. Sci.* **2012**, *27*, 585–596. [CrossRef]
27. Lončar, N.; Bar-Matthews, M.; Ayalon, A.; Surić, M.; Faivre, S. Early and Mid-Holocene environmental conditions in the Eastern Adriatic recorded in speleothems from Mala špilja Cave and Vela špilja Cave (Mljet Island, Croatia). *Acta Carsologica.* **2017**, *46*, 229–249. [CrossRef]
28. Lončar, N.; Bar-Matthews, M.; Ayalon, A.; Faivre, S.; Surić, M. Holocene Climatic Conditions in the Eastern Adriatic Recorded in Stalagmites from Strašna Peć Cave (Croatia). *Quat. Int.* **2019**, *508*, 98–106. [CrossRef]
29. Surić, M.; Columbu, A.; Lončarić, R.; Bajo, P.; Bočić, N.; Lončar, N.; Drysdale, R.N.; Hellstrom, J.C. Holocene hydroclimate changes in continental Croatia recorded in speleothem $\delta^{13}C$ and $\delta^{18}O$ from Nova Grgosova Cave. *Holocene* **2021**, *31*, 1401–1416. [CrossRef]

30. Finné, M.; Bar-Matthews, M.; Holmgren, K.; Sundqvist, H.S.; Liakopoulos, I.; Zhang, Q. Speleothem evidence for late Holocene climate variability and floods in Southern Greece. *Quat. Res.* **2014**, *81*, 213–227. [CrossRef]
31. Psomiadis, D.; Dotsika, E.; Albanakis, K.; Ghaleb, B.; Hillaire-Marcel, C. Speleothem record of climatic changes in the northern Aegean region (Greece) from the Bronze Age to the collapse of the Roman Empire. *Palaeogeogr. Palaeoclimatol. Palaeoecol.* **2018**, *489*, 272–283. [CrossRef]
32. Bar-Matthews, M.; Ayalon, A.; Kaufman, A.; Wasserburg, G.J. The Eastern Mediterranean paleoclimate as a reflection of regional events: Soreq cave, Israel. *Earth Planet. Sci. Lett.* **1999**, *166*, 85–95. [CrossRef]
33. Bar-Matthews, M.; Ayalon, A.; Gilmour, M.; Matthews, A.; Hawkesworth, C.J. Sea-land oxygen isotopic relationships from planktonic foraminifera and speleothems in the Eastern Mediterranean region and their implication for paleorainfall during interglacial intervals. *Geochim. Cosmochim. Acta* **2003**, *67*, 3181–3199. [CrossRef]
34. Bar-Matthews, M.; Ayalon, A. Mid-Holocene climate variations revealed by high resolution speleothems records from Soreq Cave, Israel and their correlation with cultural changes. *Holocene* **2011**, *21*, 163–171. [CrossRef]
35. Spötl, C.; Mangini, A.; Richards, D.A. Chronology and paleoenvironment of Marine Isotope Stage 3 from two high-elevation speleothems, Austrian Alps. *Quat. Sci. Rev.* **2006**, *25*, 1127–1136. [CrossRef]
36. Boch, R.; Cheng, H.; Spötl, C.; Edwards, R.L.; Wang, X.; Häuselmann, P. NALPS: A precisely dated European climate record 120–60 ka. *Clim. Past* **2011**, *7*, 1247–1259. [CrossRef]
37. Luetscher, M.; Lismonde, B.; Jeannin, P.-Y. Heat exchanges in the heterothermic zone of a karst system: Monlesi cave, Swiss Jura Mountains. *J. Geophys. Res.* **2008**, *113*, F02025. [CrossRef]
38. Moseley, G.E.; Spötl, C.; Svensson, A.; Cheng, H.; Brandstätter, S.; Edwards, R.L. Multi-speleothem record reveals tightly coupled climate between central Europe and Greenland during Marine Isotope Stage 3. *Geology* **2014**, *42*, 1043–1046. [CrossRef]
39. Moseley, G.E.; Spötl, C.; Cheng, H.; Boch, R.; Min, A.; Edwards, R.L. Termination-II interstadial/stadial climate change recorded in two stalagmites from the north European Alps. *Quat. Sci. Rev.* **2015**, *127*, 229–239. [CrossRef]
40. Fleitmann, D.; Cheng, H.; Badertscher, S.; Edwards, R.L.; Mudelsee, M.; Göktürk, O.M.; Fankhauser, A.; Pickering, R.; Raible, C.C.; Matter, A.; et al. Timing and climatic impact of Greenland interstadials recorded in stalagmites from northern Turkey. *Geophys. Res. Lett.* **2009**, *36*, L19707. [CrossRef]
41. McDermott, F.; Mattey, D.P.; Hawkesworth, C. Centennial-Scale Holocene Climate Variability Revealed by a High-Resolution Speleothem $\delta^{18}O$ Record from SW Ireland. *Science* **2001**, *294*, 1328–1331. [CrossRef]
42. Vansteenberge, S.; Verheyden, S.; Cheng, H.; Edwards, R.L.; Keppens, E.; Claeys, P. Paleoclimate in continental northwestern Europe during the Eemian and early Weichselian (125–97 ka): Insights from a Belgian speleothem. *Clim. Past* **2016**, *12*, 1445–1458. [CrossRef]
43. McDermott, F. Palaeo-Climate Reconstruction from Stable Isotope Variations in Speleothems: A Review. *Quat. Sci. Rev.* **2004**, *23*, 901–918. [CrossRef]
44. Fohlmeister, J.; Voarintsoa, N.R.G.; Lechleitner, F.A.; Boyd, M.; Brandtstätter, S.; Jacobson, M.J.; Oster, J.L. Main Controls on the Stable Carbon Isotope Composition of Speleothems. *Geochim. Cosmochim. Acta* **2020**, *279*, 67–87. [CrossRef]
45. Surić, M.; Juračić, M. Late Pleistocene—Holocene environmental changes—records from submerged speleothems along the Eastern Adriatic coast (Croatia). *Geol. Croat.* **2010**, *63*, 155–169. [CrossRef]
46. Surić, M.; Juračić, M.; Horvatinčić, N.; Bronić, I.K. Late Pleistocene-Holocene sea-level rise and the pattern of coastal karst inundation: Records from submerged speleothems along the Eastern Adriatic Coast (Croatia). *Mar. Geol.* **2005**, *214*, 163–175. [CrossRef]
47. Surić, M.; Horvatinčić, N.; Suckow, A.; Juračić, M.; Barešić, J. Isotope records in submarine speleothems from the Adriatic coast, Croatia. *Bull. Soc. Geol. Fr.* **2005**, *176*, 363–373. [CrossRef]
48. Surić, M.; Roller-Lutz, Z.; Mandić, M.; Bronić, I.K.; Juračić, M. Modern C, O, and H Isotope Composition of Speleothem and Dripwater from Modrič Cave, Eastern Adriatic Coast (Croatia). *Int. J. Speleol.* **2010**, *39*, 91–97. [CrossRef]
49. Surić, M.; Lončarić, R.; Lončar, N.; Buzjak, N.; Bajo, P.; Drysdale, R.N. Isotopic Characterization of Cave Environments at Varying Altitudes on the Eastern Adriatic Coast (Croatia)—Implications for Future Speleothem-Based Studies. *J. Hydrol.* **2017**, *545*, 367–380. [CrossRef]
50. Surić, M.; Lončarić, R.; Bočić, N.; Lončar, N.; Buzjak, N. Monitoring of Selected Caves as a Prerequisite for the Speleothem-Based Reconstruction of the Quaternary Environment in Croatia. *Quat. Int.* **2018**, *494*, 263–274. [CrossRef]
51. Bakrač, K.; Ilijanić, N.; Miko, S.; Hasan, O. Evidence of Sapropel S1 Formation from Holocene Lacustrine Sequences in Lake Vrana in Dalmatia (Croatia). *Quat. Int.* **2018**, *494*, 5–18. [CrossRef]
52. Ilijanić, N.; Miko, S.; Hasan, O.; Bakrač, K. Holocene Environmental Record from Lake Sediments in the Bokanjačko Blato Karst Polje (Dalmatia, Croatia). *Quat. Int.* **2018**, *494*, 66–79. [CrossRef]
53. Galović, I.; Mihalić, K.C.; Ilijanić, N.; Miko, S.; Hasan, O. Diatom Responses to Holocene Environmental Changes in a Karstic Lake Vrana in Dalmatia (Croatia). *Quat. Int.* **2018**, *494*, 167–179. [CrossRef]
54. Brunović, D.; Miko, S.; Ilijanić, N.; Peh, Z.; Hasan, O.; Kolar, T.; Miko, M.Š.; Razum, I. Holocene Foraminiferal and Geochemical Records in the Coastal Karst Dolines of Cres Island, Croatia. *Geol. Croat.* **2019**, *72*, 19–42. [CrossRef]
55. Brunović, D.; Miko, S.; Hasan, O.; Papatheodorou, G.; Ilijanić, N.; Miserocchi, S.; Correggiari, A.; Geraga, M. Late Pleistocene and Holocene paleoenvironmental reconstruction of a drowned karst isolation basin (Lošinj Channel, NE Adriatic Sea). *Palaeogeogr. Palaeoclimatol. Palaeoecol.* **2020**, *544*, 109587. [CrossRef]

56. Razum, I.; Miko, S.; Ilijanić, N.; Hasan, O.; Miko, M.Š.; Brunović, D.; Pawlowsky-Glahn, V. A compositional approach to the reconstruction of geochemical processes involved in the evolution of Holocene marine flooded coastal karst basins (Mljet Island, Croatia). *Appl. Geochem.* **2020**, *116*, 104574. [CrossRef]
57. Razum, I.; Miko, M.S.; Ilijanić, N.; Petrelli, M.; Röhl, U.; Hasan, O.; Giaccio, B. Holocene tephra record of Lake Veliko jezero, Croatia: Implications for the central Mediterranean tephrostratigraphy and sea level rise. *Boreas* **2020**, *49*, 653–673. [CrossRef]
58. Antonioli, F.; Furlani, S.; Montagna, P.; Stocchi, P. The Use of Submerged Speleothems for Sea Level Studies in the Mediterranean Sea: A New Perspective Using Glacial Isostatic Adjustment (GIA). *Geosciences* **2021**, *11*, 77. [CrossRef]
59. Toucanne, S.; Minto'o, C.M.A.; Fontanier, C.; Bassetti, M.-A.; Jorry, S.J.; Jouet, G. Tracking rainfall in the northern Mediterranean borderlands during sapropel deposition. *Quat. Sci. Rev.* **2015**, *129*, 178–195. [CrossRef]
60. Peel, M.C.; Finlayson, B.L.; McMahon, T.A. Updated World Map of the Köppen-Geiger Climate Classification. *Hydrol. Earth Syst. Sci.* **2007**, *11*, 1633–1644. [CrossRef]
61. Luetscher, M.; Boch, R.; Sodemann, H.; Spötl, C.; Cheng, H.; Edwards, R.L.; Frisia, S.; Hof, F.; Müller, W. North Atlantic Storm Track Changes during the Last Glacial Maximum Recorded by Alpine Speleothems. *Nat. Commun.* **2015**, *6*, 6344. [CrossRef]
62. *CMHS (2021)*; Croatian Meteorological and Hydrological Service: Zagreb, Croatia, 2021.
63. Surić, M.; Czuppon, G.; Lončarić, R.; Bočić, N.; Lončar, N.; Bajo, P.; Drysdale, R.N. Stable Isotope Hydrology of Cave Groundwater and Its Relevance for Speleothem-Based Paleoenvironmental Reconstruction in Croatia. *Water* **2020**, *12*, 2386. [CrossRef]
64. Hellstrom, J. Rapid and accurate U/Th dating using parallel ion-counting multi-collector ICP-MS. *J. Anal. At. Spectrom.* **2003**, *18*, 1346–1351. [CrossRef]
65. Drysdale, R.N.; Paul, B.T.; Hellstrom, J.C.; Couchoud, I.; Greig, A.; Bajo, P.; Zanchetta, G.; Isola, I.; Spötl, C.; Baneschi, I.; et al. Precise microsampling of poorly laminated speleothems for U-series dating. *Quat. Geochronol* **2012**, *14*, 38–47. [CrossRef]
66. Hellstrom, J. U–Th dating of speleothems with high initial ^{230}Th using stratigraphical constraint. *Quat. Geochronol.* **2006**, *1*, 289–295. [CrossRef]
67. Hua, Q.; Jacobsen, G.E.; Zoppi, U.; Lawson, E.M.; Williams, A.A.; Smith, A.M.; McGann, M.J. Progress in radiocarbon target preparation at the ANTARES AMS centre. *Radiocarbon* **2001**, *43*, 275–282. [CrossRef]
68. Fink, D.; Hotchkis, M.; Hua, Q.; Jacobsen, G.; Smith, A.M.; Zoppi, U.; Child, D.; Mifsud, C.; van der Gaast, H.; Williams, A.; et al. The Antares AMS facility at ANSTO. *Nucl. Instrum. Methods Phys. Res. B* **2004**, *223*, 109–115. [CrossRef]
69. Tremaine, D.M.; Froelich, P.N.; Wang, Y. Speleothem calcite farmed in situ: Modern calibration of δ^{18}O and δ^{13}C paleoclimate proxies in a continuously-monitored natural cave system. *Geochim. Cosmochim. Acta* **2011**, *75*, 4929–4950. [CrossRef]
70. Cheng, H.; Edwards, R.L.; Shen, C.-C.; Polyak, V.J.; Asmerom, Y.; Woodhead, J.; Hellstrom, J.; Wang, Y.; Kong, X.; Spötl, C.; et al. Improvements in ^{230}Th dating, ^{230}Th and ^{234}U half-life values, and U-Th isotopic measurements by multi-collector inductively coupled plasma mass spectrometry. *Earth Planet. Sci. Lett.* **2013**, *371–372*, 82–91. [CrossRef]
71. Hendy, E.J.; Tomiak, P.J.; Collins, M.J.; Hellstrom, J.; Tudhope, A.W.; Lough, J.M.; Penkman, K.E.H. Assessing amino acid racemization variability in coral intra-crystalline protein for geochronological applications. *Geochim. Cosmochim. Acta* **2012**, *86*, 338–353. [CrossRef]
72. Scholz, D.; Hoffmann, D.L.; Hellstrom, J.; Ramsey, C.B. A comparison of different methods for speleothem age modelling. *Quat. Geochronol.* **2012**, *14*, 94–104. [CrossRef]
73. Bajo, P.; Drysdale, R.N.; Woodhead, J.D.; Hellstrom, J.C.; Hodell, D.; Ferretti, P.; Voelker, A.H.L.; Zanchetta, G.; Rodrigues, T.; Wolff, E.; et al. Persistent influence of obliquity on ice age terminations since the Middle Pleistocene transition. *Science* **2020**, *367*, 1235–1239. [CrossRef] [PubMed]
74. Bajo, P.; Hellstrom, J.; Frisia, S.; Drysdale, R.; Black, J.; Woodhead, J.; Borsato, A.; Zanchetta, G.; Wallace, M.W.; Regattieri, E.; et al. "Cryptic" diagenesis and its implications for speleothem geochronologies. *Quat. Sci. Rev.* **2016**, *148*, 17–28. [CrossRef]
75. Griffiths, M.L.; Fohlmeister, J.; Drysdale, R.N.; Hua, Q.; Johnson, K.R.; Hellstrom, J.C.; Gagan, M.K.; Zhao, J.-X. Hydrological control of the dead carbon fraction in a Holocene tropical speleothem. *Quat. Geochronol.* **2012**, *14*, 81–93. [CrossRef]
76. Bajo, P.; Borsato, A.; Drysdale, R.; Hua, Q.; Frisia, S.; Zanchetta, G.; Hellstrom, J.; Woodhead, J. Stalagmite carbon isotopes and dead carbon proportion (DCP) in a near-closed-system situation: An interplay between sulphuric and carbonic acid dissolution. *Geochim. Cosmochim. Acta* **2017**, *210*, 208–227. [CrossRef]
77. Hua, Q.; Cook, D.; Fohlmeister, J.; Penny, D.; Bishop, P.; Buckmann, S. Radiocarbon dating of a speleothem record of paleoclimate for Angkor, Cambodia. *Radiocarbon* **2017**, *59*, 1873–1890. [CrossRef]
78. Frisia, S.; Borsato, A.; Fairchild, I.J.; Susini, J. Variations in atmospheric sulphate recorded in stalagmites by synchrotron micro XRF and XANES analyses. *Earth Planet. Sci. Lett.* **2005**, *235*, 729–740. [CrossRef]
79. Scholz, D.; Frisia, S.; Borsato, A.; Spötl, C.; Fohlmeister, J.; Mudelsee, M.; Miorandi, R.; Mangini, A. Holocene climate variability in north-eastern Italy: Potential influence of the NAO and solar activity recorded by speleothem data. *Clim. Past* **2012**, *8*, 1367–1383. [CrossRef]
80. Regattieri, E.; Zanchetta, G.; Isola, I.; Bajo, P.; Perchiazzi, N.; Drysdale, R.N.; Boschi, C.; Hellstrom, J.C.; Francke, A.; Wagner, B. A MIS 9/MIS 8 speleothem record of hydrological variability from Macedonia (F.Y.R.O.M.). *Glob. Planet. Chang.* **2018**, *162*, 39–52. [CrossRef]
81. Fairchild, I.J.; Borsato, A.; Tooth, A.F.; Frisia, S.; Hawkesworth, C.J.; Huang, Y.; McDermott, F.P.; Spiro, B. Controls on trace element (Sr-Mg) compositions of carbonate cave waters: Implications for speleothem climatic records. *Chem. Geol.* **2000**, *166*, 255–269. [CrossRef]

82. Martín-Chivelet, J.; Muñoz-García, M.B.; Cruz, J.A.; Ortega, A.I.; Turrero, M.J. Speleothem Architectural Analysis: Integrated approach for stalagmite-based paleoclimate research. *Sediment. Geol.* **2017**, *353*, 28–45. [CrossRef]
83. Dreybrodt, W. Chemical kinetics, speleothem growth and climate. *Boreas* **1999**, *28*, 347–356. [CrossRef]
84. Railsback, L.B.; Liang, F.Y.; Romani, J.R.V.; Grandal-d'Anglade, A.; Rodríguez, M.V.; Fidalgo, L.S.; Mosquera, D.F.; Cheng, H.; Edwards, R.L. Petrographic and isotopic evidence for Holocene long-term climate change and shorter-term environmental shifts from a stalagmite from the Serra do Courel of northwestern Spain, and implications for climatic history across Europe and the Mediterranean. *Palaeogeogr. Palaeoclimatol. Palaeoecol.* **2011**, *305*, 172–184. [CrossRef]
85. Genty, D.; Quinif, Y. Annually laminated sequences in the internal structure of some Belgian stalagmites—importance for paleoclimatology. *J. Sediment. Res.* **1996**, *66*, 275–288. [CrossRef]
86. Muñoz-García, M.B.; Cruz, J.; Martín-Chivelet, J.; Ortega, A.I.; Turrero, M.J.; López-Elorza, M. Comparison of speleothem fabrics and microstratigraphic stacking patterns in calcite stalagmites as indicators of paleoenvironmental change. *Quat. Int.* **2016**, *407*, 74–85. [CrossRef]
87. Regattieri, E.; Isola, I.; Zanchetta, G.; Drysdale, R.N.; Hellstrom, J.C.; Baneschi, I. Stratigraphy, petrography and chronology of speleothem deposition at Tana che Urla (Lucca, Italy): Paleoclimatic implications. *Geogr. Fis. Din. Quat.* **2012**, *35*, 141–152. [CrossRef]
88. Keith, M.L.; Weber, J.N. Carbon and oxygen isotopic composition of selected limestones and fossils. *Geochim. Cosmochim. Acta* **1964**, *28*, 1787–1816. [CrossRef]
89. Spötl, C.; Fohlmeister, J.; Cheng, H.; Boch, R. Modern aragonite formation at near-freezing conditions in an alpine cave, Carnic Alps, Austria. *Chem. Geol.* **2016**, *435*, 60–70. [CrossRef]
90. Sarıkaya, M.A.; Stepišnik, U.; Žebre, M.; Çiner, A.; Yıldırım, C.; Vlahović, I.; Tomljenović, B.; Matoš, B.; Wilcken, K.M. Last glacial maximum deglaciation of the Southern Velebit Mt. (Croatia): Insights from cosmogenic ^{36}Cl dating of Rujanska Kosa. *Mediterr. Geosci. Rev.* **2020**, *2*, 53–64. [CrossRef]
91. Krklec, K.; Domínguez-Villar, D.; Perica, D. Depositional environments and diagenesis of a carbonate till from a Quaternary paleoglacier sequence in the Southern Velebit Mountain (Croatia). *Palaeogeogr. Palaeoclimatol. Palaeoecol.* **2015**, *436*, 188–198. [CrossRef]
92. Štefanec, N. Trgovina drvetom na Triplex Confiniumu ili kako izvući novac iz senjskih šuma (1600–1630)? (Wood Trade on the Triplex Confinium or How to Extract Money from Senj Woodlands (1600–1630)?). In *Triplex Confinium (1500.–1800.): Ekohistorija*; Zavod za Hrvatsku Povijest Filozofskog Fakulteta Sveučilišta u Zagrebu: Zadar, Croatia, 2000; pp. 337–365. (In Croatian)
93. Kaser, K. Uništenje šuma na obalnom kraškom području hrvatske Vojne krajine u prvoj polovici 18. stoljeća. Njegovi demografski, privredni i socijalni uzroci. (Destruction of forests in the coastal karst area of the Croatian Military Border in the first half of the 18th century. Its demographic, economic and social causes). In *Historijski Zbornik 40*; Kampuš, I., Ed.; Savez Povijesnih Društava Hrvatske: Zagreb, Croatia, 1987; pp. 121–137. (In Croatian)
94. Dumitru, O.A.; Onac, B.P.; Polyak, V.J.; Wynn, J.G.; Asmerom, Y.; Fornós, J.J. Climate variability in the western Mediterranean between 121 and 67 ka derived from a Mallorcan speleothem record. *Palaeogeogr. Palaeoclimatol. Palaeoecol.* **2018**, *506*, 128–138. [CrossRef]
95. Rogerson, M.; Dublyansky, Y.; Hoffmann, D.L.; Luetscher, M.; Töchterle, P.; Spötl, C. Enhanced Mediterranean water cycle explains increased humidity during MIS 3 in North Africa. *Clim. Past* **2019**, *15*, 1757–1769. [CrossRef]
96. Horvatinčić, N.; Bronić, I.K.; Barešić, J.; Obelić, B.; Vidič, S. Tritium and stable isotope distribution in the atmosphere at the coastal region of Croatia. In *Isotopic Composition of Precipitation in the Mediterranean Basin in Relation to Air Circulation Patterns and Climate*; IAEA-TECDOC-1453; Gourcy, L., Ed.; IAEA: Vienna, Austria, 2005; pp. 37–50.
97. Krajcar Bronić, I.; Vreča, P.; Horvatinčić, N.; Barešić, N.; Obelić, N. Distribution of hydrogen, oxygen and carbon isotopes in the atmosphere of Croatia and Slovenia. *Arh. Hig. Rada Toksiko.* **2006**, *57*, 23–29.
98. Vreča, P.; Bronić, I.K.; Horvatinčić, N.; Barešić, J. Isotopic Characteristics of Precipitation in Slovenia and Croatia: Comparison of Continental and Maritime Stations. *J. Hydrol.* **2006**, *330*, 457–469. [CrossRef]
99. Barešić, J.; Horvatinčić, N.; Bronić, I.K.; Obelić, B.; Vreča, P. Stable Isotope Composition of Daily and Monthly Precipitation in Zagreb. *Isot. Environ. Health Stud.* **2006**, *42*, 239–249. [CrossRef]
100. Drysdale, R.N.; Zanchetta, G.; Hellstrom, J.C.; Fallick, A.E.; McDonald, J.; Cartwright, I. Stalagmite evidence for the precise timing of North Atlantic cold events during the early last glacial. *Geology* **2007**, *35*. [CrossRef]
101. Surić, M.; Richards, D.A.; Hoffmann, D.L.; Tibljaš, D.; Juračić, M. Sea-level change during MIS 5a based on submerged speleothems from the eastern Adriatic Sea (Croatia). *Mar. Geol.* **2009**, *262*, 62–67. [CrossRef]
102. Waelbroeck, C.; Labeyrie, L.; Michel, E.; Duplessy, J.C.; McManus, J.F.; Lambeck, K.; Balbon, E.; Labracherie, M. Sea-level and deep water temperature changes derived from benthic foraminifera isotopic records. *Quat. Sci. Rev.* **2002**, *21*, 295–305. [CrossRef]
103. Goni, M.S.; Eynaud, F.; Turon, J.L.; Shackleton, N.J. High resolution palynological record off the Iberian margin: Direct land-sea correlation for the Last Interglacial complex. *Earth Planet. Sci. Lett.* **1999**, *171*, 123–137. [CrossRef]
104. Dorale, J.A.; Liu, Z. Limitations of Hendy Test criteria in judging the paleoclimatic suitability of speleothems and the need for replication. *J. Cave Karst Stud.* **2009**, *71*, 73–80.
105. Mickler, P.J.; Banner, J.L.; Stern, L.; Asmerom, Y.; Edwards, R.L.; Ito, E. Stable isotope variations in modern tropical speleothems: Evaluating equilibrium vs. kinetic isotope effects. *Geochim. Cosmochim. Acta* **2004**, *68*, 4381–4393. [CrossRef]
106. Gascoyne, M. Palaeoclimate determination from cave calcite deposits. *Quat. Sci. Rev.* **1992**, *11*, 609–632. [CrossRef]